공학박사학위논문

나무 물관 내부 공동 현상에 대한 유체역학적 분석

Hydrodynamic analysis of cavitation inside wood xylem

2019년 8월

서울대학교 대학원

기계항공공학부

최 진 우

Abstract

Hydrodynamic analysis of cavitation inside wood xylem

Jin Woo Choi
Department of Mechanical and Aerospace Engineering
The Graduate School
Seoul National University

A dry environment is fatal to plants. If water is not supplied properly, cavitation happens inside the stem and the bubble blocks the xylem. This is called embolism. When embolism occurs, roots cannot supply enough water to hydrate mesophylls in leaves. The process of embolization can be divided into two processes: the propagation of the air bubble from the gas-filled vessel element to the adjacent, and the growing of the bubble until it fills the element. In this study, synthetic tree experiments elucidated the mechanics of embolization, and the results were applied to actual biological data.

The synthetic tree is the model system which contains a bulk volume of water surrounded by a porous media. In porous media, the interface of the water pulls the volume of water, so negative pressure is generated. When the magnitude of the negative pressure exceeds beyond the threshold, cavitation happens in the bulk volume of water. Experimental results show that: 1) As the volume of bulk water increases, the volumetric change of the synthetic

tree until the cavitation increases. That is, the hydraulic capacitance of the synthetic tree is increased. 2) As the temperature decreases, the cavitation threshold increases. As a result, the pressure difference before cavitation with the outside can be increased, and the membrane fracture can happen. After cavitation, 3) the bubble with a low threshold pressure near zero increases its size at a slow and constant speed (Darcy expansion). 4) The bubble with a high threshold pressure has fast initial speed but it decelerates its speed (poroelastic expansion).

The embolism resistance of a plant stem is determined by the anatomy of the stem. In this study, we classified its components into woods, parenchyma cells, and empty spaces (lumen). In the plane of lumen fraction and embolism resistivity, the regime of plant shows that 1) as the ratio of lumen fraction decreases, capacitance decreases, the bubble is formed rapidly, and embolism resistance decreases. 2) The larger lumen fraction, the greater the possibility of fracture on the vessel wall, thus it reduces the embolism resistance. 3) Two strategies for increasing embolism resistance are distinguished from angiosperms and gymnosperms. Since angiosperms live in a high-temperature environment, cavitation can occur frequently, and parenchyma fraction is increased to cope with embolism. Because gymnosperms live in low-temperature environments, bubbles are less likely to form and fractures can occur on the vessel wall because of a large pressure difference. Thus, gymnosperms increase the strength of the vessel wall against fracture.

Keyword : Cavitation, Embolism, Implosion, Embolism resistivity

Student Number : 2014-21843

Table of Contents

List of Figures

Figure 2.5. (a) The weight change of synthetic tree, Δm, of different water drop diameter d. (b) Analytically, the weight change converges to Δm_{e}; however, it ends at Δm_{c} because of cavitation. Here $D = 20$ mm, $H = 2$ mm, heating temperature $T = 80°\mathrm{C}$, and Δm_{e} is 45 mg.

Figure 2.6. The weight change drastically decreases after cavitation because $-\Delta P \approx -P_{\mathrm{LV}}$ is much higher than before $-\Delta P = -P_{\mathrm{L},i} + P_{\mathrm{L}}$.

Figure 2.7. (a) Normalized volume loss until cavitation follows $(d/D)^{3/2}$. The volume change until cavitation increased with lower temperatures because it decreased the cavitation pressure. (b) Implosion rate of the synthetic trees increased in low heating temperature because of high pressure difference. $d = 20$ mm, $H = 2$ mm (•) and $d = 10$ mm, $H = 1.4$ mm (▪)

Figure 2.8. Schematic images of the synthetic tree which are made by putting together flat and engraved hydrogel sheets. It contains ten aligned bulk cavity filled with water.

Figure 2.9. A double molding technique was used to fabricate the engraved hydrogel. The pre-cured engraved and flat hydrogel was put together and irradiated UV light (385 nm) for an extra 30 seconds to fully polymerize. Then, the hydrogel was soaked in $95°\mathrm{C}$ water for two days to fill water and to remove chemical residues.

Figure 2.10. (a) Schematic image of physical vapor deposition (PVD) of trichlorosilane on the primary mold. (b) Optical microscopy image of bumps generation after PVD for 60 s and 600 s. (c) Atomic force microscopy scanning image of bumps after PVD for 600 s.

Figure 2.11. (a) Actual image of the synthetic in the cage. Two holes are to control the evaporating area. (b) The magnified image of the synthetic tree after cavitation (c) the optical microscope image of the synthetic tree after cavitation.

Figure 2.12. Two types of bubble expansion were observed. The speed of the bubble in the poroelastic expansion is fast but decelerated, and the speed of

Chapter 1. Introduction

1.1. The vascular system of large organisms

If there is something in common with larger creatures, it is developing vascular systems (Labarbera, 1990; McCulloh, Sperry, & AdlerO, 2004). This is because delivering materials with the flow, a process known as advection, is much more effective than depending on random distribution driven by concentration difference, which is diffusion. This inversion can be expressed by Peclet number:

$$\mathrm{Pe}_L = \left(\frac{u}{L}\right)\left(\frac{L^2}{D}\right) = \frac{Lu}{D} \tag{1.1}$$

Here L is the size of the organism, u is the flow-speed inside the organism, and D is the diffusion coefficient of the liquid media. That is, Peclet number is the fraction of the delivering rate by advection, u/L, over the rate by diffusion, D/L^2. Thus a vascular system with the flow is effective when $\mathrm{Pe}_L \gg 1$. Small plants such as moss do not have to construct the vascular system for advection; however, woody plants such as trees and shrubs have to manufacture the system consisting of xylem and phloem.

A plant needs lots of water. It absorbs liquid water and desorbs water vapor to intake carbon dioxide (Figure 1.1a). That is not because water is needed for the photosynthetic process: $\mathrm{light} + 6\mathrm{H_2O} + 6\mathrm{CO_2} \rightarrow \mathrm{C_6H_{12}O_6} + 6\mathrm{O_2}$, but because the plant exchanges water for carbon dioxide.

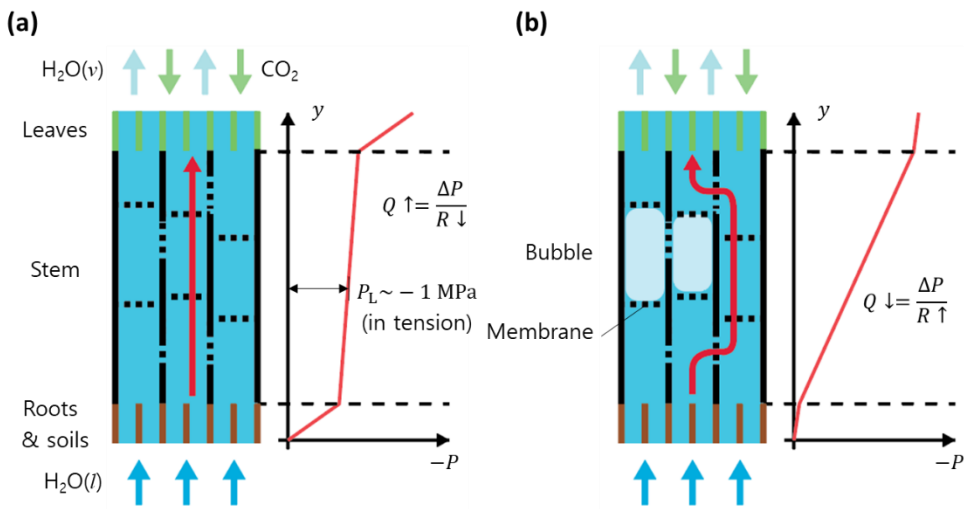

Figure 1.1. (a) Plants absorb liquid water and desorb water vapor to take in carbon dioxide for photosynthesis. Plants with high Peclet numbers have evolved a vascular system which consists of vessel elements and pit membranes, which can capture cavitation bubbles. (b) After cavitation happens, the bubble blocks the conduit and makes hydraulic resistance increase, which is embolism.

However, their water use efficiency is very low, ranging between 0.5-10 mmol of carbon dioxide intake per mol of water molecule evaporation (Nobel, 1991). Thus the large plants should construct the "water highway" which is made of dead cell wall skeletons: xylem. The flow-speed inside xylem is about $10^{-3}\ \mathrm{m/s}$ with some inorganic nutrients from the roots to the leaves and growth tissues. In contrast, it is enough to construct the "small country road" made of living cells passing through the village: phloem. The flow speed inside the phloem is about $10^{-4}\ \mathrm{m/s}$ while transporting the organic nutrient, which is the product of photosynthesis (Jensen et al., 2016). Despite the flow inside plants being passive, the vascular water transport has been termed the "backbone of plant physiology (Brodribb, 2009)."

The flow rate inside the vascular system is driven by pressure difference:

$$Q = \frac{\Delta P}{R} \tag{1.2}$$

Here Q is the volumetric flow rate inside the vascular system $[\mathrm{m^3/s}]$, ΔP is the pressure difference [MPa], and R is the hydraulic resistance $[\mathrm{m^{-3}s\ MPa}]$. To supply enough water from the soil to leaves, angiosperms have evolved to have conduits with a larger diameter, which are vessels, than that of gymnosperms, which are tracheids, in order to decrease hydraulic resistance. To increase pressure difference, animals pump their blood by means of beating their heart; however, plants use passively generated pressure difference driven by moisture contents of the surrounding atmosphere.

1.2. Negative pressure driven by surface tension

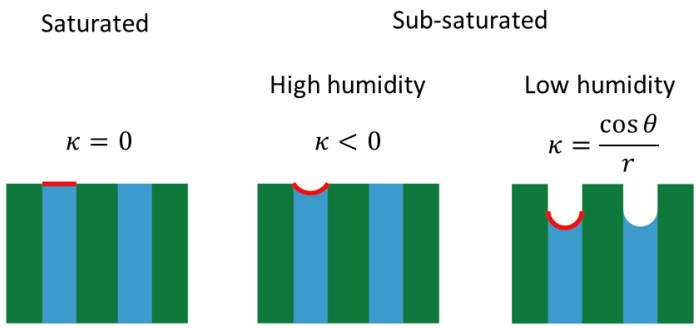

Figure 1.2. If the atmosphere is saturated with water vapor, the interface is flat, $\kappa = 0$. The interface becomes concave, $\kappa = 0$, if it is unsaturated. If the relative humidity is low, the curvature of the interface is determined by material properties. θ is contact angle and r is pore size.

A cup of water should always evaporate into the air until the air is saturated with water vapor. The microscopic interface, instead, can balance with an unsaturated atmosphere with large curvature (Figure 1.2). The curvature of the interface is determined by the Kelvin equation:

$$\gamma\kappa = \frac{RT}{v_w}\ln\left(\frac{w}{w_{\text{sat}}}\right) \tag{1.3}$$

Here γ is the surface tension coefficient of water, κ is the curvature of the interface, RT is thermal energy, v_w is the molar volume of liquid water, and w/w_{sat} is the relative humidity of air near the interface. The sub-saturated air makes the interface concave ($\kappa < 0$).

On the other hand, the interface needs to flatten its curvature to minimize surface free energy, a process described by cohesion-tension theory (Dixon & Joly, 1894). That tendency derives Laplace pressure which is the pressure

difference between atmospheric pressure and the hydrostatic pressure beneath the interface, namely interfacial pressure, $P_{\mathrm{L},i}$ (De Gennes, Brochard-Wyart, & Quéré, 2013):

$$\gamma\kappa = P_{\mathrm{L},i} - P_0 \tag{1.4}$$

Here, $P_{\mathrm{L},i}$ is the interfacial pressure and P_0 is the atmospheric pressure, which is 100 kPa. If the curvature, in case of water, is less than $-P_0/\gamma$ or the radius of curvature is less than 1 μm, the interfacial pressure becomes negative. Typical cell wall pores in the leaves can generate an interfacial pressure of -10 to -100 MPa (for 10 nm and 1 nm respectively).

1.3. Cavitation and embolism in xylem

Liquid water in negative pressure is thermodynamically metastable because water at $20°\mathrm{C}$ boils at an absolute pressure of 2.3 kPa. Nonetheless, boiling can be avoided if we reduce nucleation sites, such as small air bubbles, impurities, and irregular contact zones. However, a lower negative pressure limit eventually exists where cavitation will occur, P_{c}, which is around -1 MPa in plant xylem. A bubble from cavitation in negative pressure always obstructs a conduit of the vascular system, which is air embolism (Figure 1.1b). This is because the gas bubble cannot maintain the negative pressure since the intermolecular distance is farther than liquid or solid. Therefore, the pressure of the water around the bubble is close to zero. Then, the water from the periphery of the bubble flows outward according to the pressure gradient. In other words, the bubble expands the size.

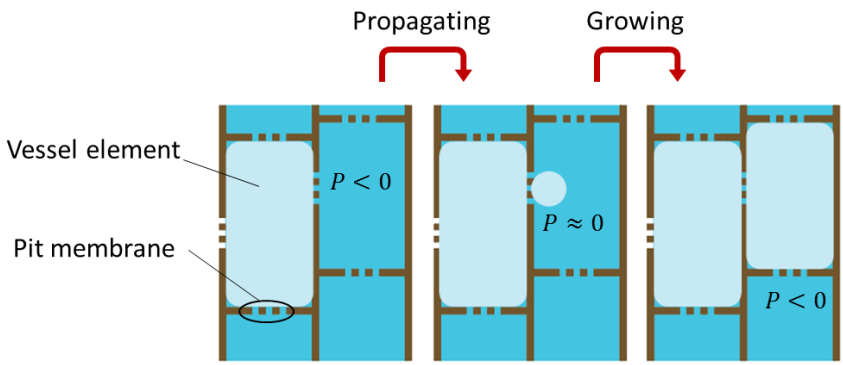

Figure 1.3. Plants are more fatal to air embolism than animals because the bubble grows its size in tension, and then it propagates to an adjacent vessel element. The process increases hydraulic resistance.

Fortunately, plant vessels are compartmented into vessel elements rather than the bundle of independent tubes, with each vessel element separated by pit membranes (Figure 1.3). The membrane permeates water but delays the inflow of air. After a bubble fills the vessel element, water detours to the leaves with the increased hydraulic resistance in equation 1.2. Repeating this step of embolization in drought conditions, roots cannot supply enough water to hydrate the leaves, which is lethal to the survival of the plant (Brendan Choat et al., 2018).

1.4. Purpose of Research

The purpose of this study is to mechanically explain the process of embolization in the plant vascular system. The hydraulic resistance of the plant stem increases as the bubble propagates from the adjacent vessel element and fills the other vessel element. In other words, the embolization can be classified into two processes: propagation of a bubble and growth of the bubble (Figure 1.3). Delaying the process of embolization is an important

factor for inhabitation especially a dry environment.

In Chapter 2, we devised two model systems, which are synthetic trees, to explore the process of embolization. About the propagation of a bubble, we measured the mass change of the synthetic tree until the cavitation happens. It is to describe the hydraulic capacitance until cavitation happens. We also found the relationship between the cavitation pressure and temperature, and its impact on the solid surroundings. Regarding the growing of the bubble, we investigated the length variation of the cavitation bubble in narrow voids. We determined the interfacial pressure, $P_{\mathrm{L},i}$, and cavitation pressure, P_{c}, which drive the dynamics of the bubble expansion in the channels inside porous media by measuring the speed of the bubble growth.

In chapter 3, the actual plant data was analyzed based on the results of experiments. The parameters that can represent the cavitation resistance and the anatomical characteristics of the plant stem were selected and the values according to the plant species were collected in the previous studies. Based on these results, it was confirmed that the anatomical structure of the plant stem was restricted in order to increase the embolism resistance. The boundaries were mechanically analyzed.

Chapter 2. Synthetic tree experiments

2.1. Synthetic tree and its surrounding pressures

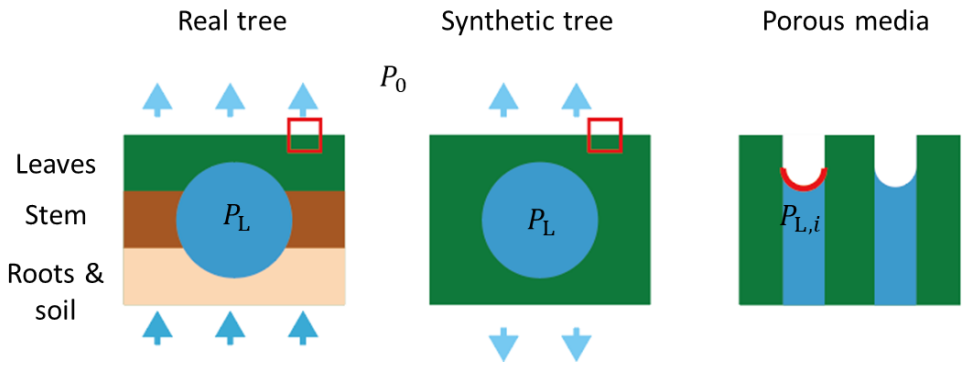

Figure 2.1. A tree contains bulk water surrounded by porous media. In case of real tree, porous media is mesophyll cells in leaves and the soil adjacent to its roots. P_0 is atmospheric pressure, P_L is liquid pressure, and $P_{L,i}$ is interfacial pressure determined by equation 2.1.

The synthetic tree is the bulk volume of water surrounded by wetted porous media (Vincent, Marmottant, Quinto-Su, & Ohl, 2012; Wheeler & Stroock, 2008) (Figure 2.1). In the real tree, the upper porous media is mesophyll in the leaves and lower porous media is the soil next to roots (Table 2.1). The curvature in the liquid-air interface is determined by equation 1.3. However,

Table 2.1. Similarities between the real tree and the synthetic tree.

	Real tree	Synthetic tree
(1) Porous media	Mesophyll cell, soil	Hydrogel (or PDMS)
(2) Bulk water	In xylem	In bulk cavity

if the relative humidity is too low or pore size is too large, the magnitude of the curvature is restricted to $\cos\theta_{\mathrm{R}}/r$. Here θ_{R} is receding contact angle and r is pore size. At this time, the interface retreats into porous media (Figure 1.2). Thus, the interfacial pressure is determined by the equation as below:

$$P_{\mathrm{L},i} = P_0 - \min\left[-\frac{RT}{v_w}\ln\left(\frac{w}{w_{\mathrm{sat}}}\right), \frac{\gamma\cos\theta_{\mathrm{R}}}{r}\right] \tag{2.1}$$

Thus, the interfacial pressure is determined by the material properties of porous media if the relative humidity is low enough. Fornasiero et al. found that flowrate inside poly(hydroxyethyl methacrylate) (pHEMA) is almost the same if the relative humidity is below 85% (Fornasiero, Tang, Boushehri, Prausnitz, & Radke, 2008), which is equal to -20 MPa on the interfacial pressure. With similar methods, Vincent et al. evaluated the interface pressure of -100 MPa in porous silicon of 3 nm pore size below 50% relative humidity (Vincent, Szenicer, & Stroock, 2016).

Bulk liquid water in negative pressure is mechanically stable ($\partial P_{\mathrm{L}}/\partial V < 0$, P_{L} is the bulk pressure and V is the volume of bulk liquid water) but thermodynamically metastable with respect to water vapor (Debenedetti, 1996). Wheeler & Stroock confined the water with a pHEMA to provide stable liquid water of -20 MPa at 85% relative humidity, but cavitation occurred at drier atmosphere (Wheeler & Stroock, 2008). Vincent et al. observed the expansion of liquid water until the cavitation in the same hydrogel, and calculated the cavitation pressure, P_{c}, of -30 MPa by applying the bulk modulus of water, which is 2.2 GPa (Vincent et al., 2012).

Hubert et al. focused high amplitude sound wave in the bulk liquid water, and obtained the cavitation pressure of -27 MPa at 0°C to -17 MPa at 80°C (Herbert, Balibar, & Caupin, 2006). Thus, bulk water can experimentally endure tens of MPa range in negative pressure before cavitation.

2.2. Fabrication of deformable synthetic tree

Bulk liquid water of spherical-cap-shape surrounded by poly (dimethylsiloxane) (PDMS) was adopted as the synthetic tree (Figure 2.2). PDMS was selected as the porous media because of its extremely high permeability to water vapor (Berthier, Young, & Beebe, 2012). Noblin et al. used PDMS synthetic tree to describe the optimal venation of plant leaves (Noblin et al., 2008). Because of the low elastic modulus of PDMS, which is 2.6 MPa at 10:1 curing ratio (Wang, Volinsky, & Gallant, 2014), we confined it in a rigid acrylic container and a thin plate to restrict the extent of deformation. We used Whatman® Anodisc inorganic filter (anodized aluminum oxide, AAO) membrane of 0.1 μm pore size as the thin plate. Water vapor only evaporates through the AAO membrane, not the acrylic.

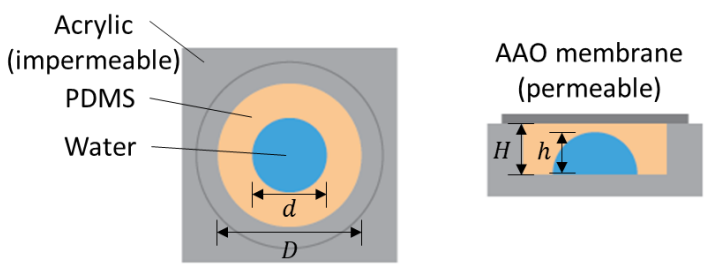

Figure 2.2. Schematic images of the deformable synthetic tree. The bulk volume of water and surrounding porous media is confined in a solid substrate. During evaporation, the AAO membrane concavely deforms.

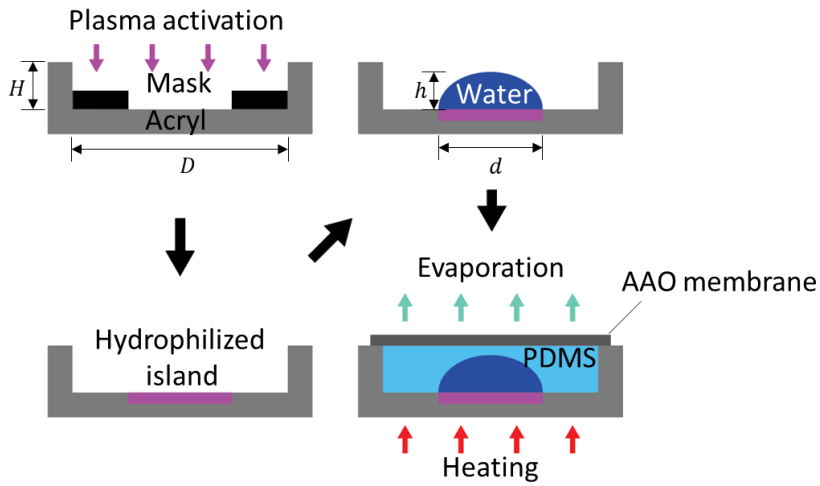

Figure 2.3. The fabrication process of the deformable synthetic tree. To set the diameter of water droplet d, plasma activation was treated to hydrophilize the substrate below the water droplet.

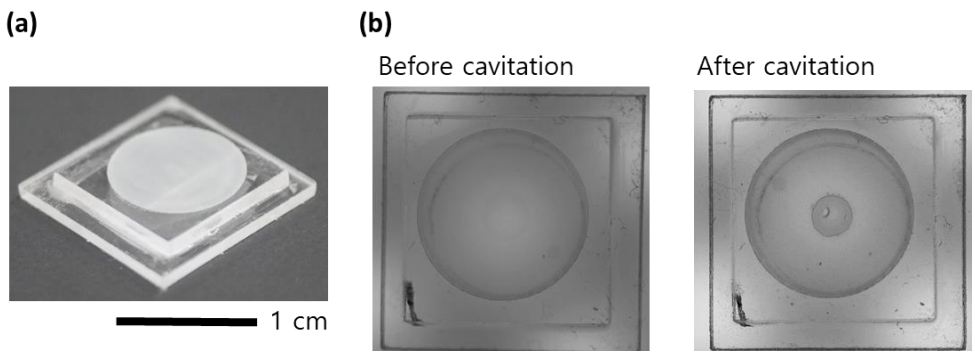

Figure 2.4. (a) the final shape of the synthetic tree. (b) image of the synthetic tree before and after cavitation.

The process in detail is as follows (Figure 2.3): First, an acrylic container of inner diameter D and height H was fabricated with one end opened. A plastic tape (3M 471) with punctured diameter d was attached inside the container. Then, plasma activation is performed to give a hydrophilic island of diameter d. After detaching the tape, the exact volume of water, V, was applied by micropipette to match the height of the droplet, h, to $0.9H$. Here, $V = \frac{1}{6}\pi h\left(\frac{3}{4}d^2 + h^2\right)$. Then, we slightly applied pre-cured PDMS with the flow rate of 0.2 ml/min using Longer Pump® syringe pump in the remaining space and covered it with the anodized aluminum oxide (AAO) membrane. Figure 2.4a is the final shape of the synthetic tree. The synthetic tree was heated and mass change with time was measured. We could optically check whether cavitation happens or not (Figure 2.4b).

2.3. Mass change of synthetic tree

During the mass of the synthetic tree, m, decreases due to evaporation, the pressure of bulk water, P_{L}, also decreases. The change can be expressed using the hydraulic capacitance of the synthetic tree, C (Nobel, 1983):

$$\Delta m = \rho C(P_{\mathrm{L}} - P_0) \tag{2.2}$$

Δm is the mass change, ρ is the density of water, and P_0 is the atmospheric pressure. The weight change of the synthetic tree with time follows Darcy's equation:

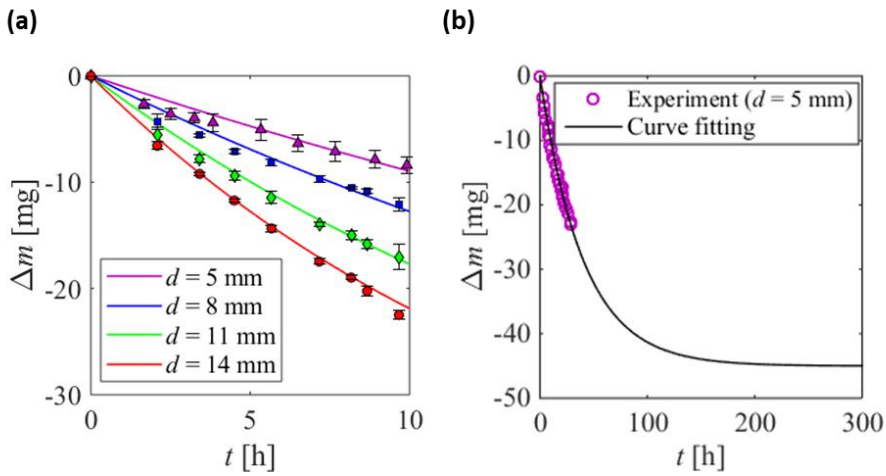

Figure 2.5. (a) The weight change of synthetic tree, Δm, of different water drop diameter d. (b) Analytically, the weight change converges to Δm_{e}; however, it ends at Δm_{c} because of cavitation. Here $D = 20$ mm, $H = 2$ mm, heating temperature $T = 80°\mathrm{C}$, and Δm_{e} is 45 mg.

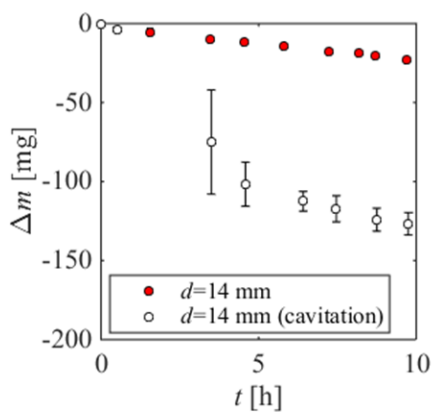

Figure 2.6. The weight change drastically decreases after cavitation because $-\Delta P \approx -P_{\mathrm{LV}}$ is much higher than before $-\Delta P = -P_{\mathrm{L},i} + P_{\mathrm{L}}$.

$$\frac{\mathrm{d}m}{\mathrm{d}t} = \rho \frac{\Delta P}{R} \tag{2.3}$$

ΔP is $P_{\mathrm{L},i} - P_{\mathrm{L}}$, R is hydraulic resistance. We can assume $P_{\mathrm{L},i}$ is constant because of the dry atmosphere by equation 2.1.

Using equation 2.2 and 2.3, the weight change of the synthetic tree over time can be expressed as follow:

$$\mathrm{m}(t) = m_0 - \Delta m_{\mathrm{e}}\left(1 - e^{-t/\tau}\right) \tag{2.4}$$

m_0 is the initial mass of the synthetic tree, Δm_{e} is the amount of mass change until equilibrium, $\rho C(P_{\mathrm{V}} - P_{\mathrm{L},i})$, and τ is the time constant RC. That is, the mass of the synthetic tree decreases fast if the time constant is low (Figure 2.5a). On the other hand, the weight change cannot converge to the equilibrium weight change, Δm_{e} because of cavitation (Figure 2.5b). when a bubble is formed, the liquid pressure P_{L} becomes zero, so that the flow rate increases (Figure 2.6). Here, flowrate change is considerable, so we can assume that $P_{\mathrm{L},i} \ll P_{\mathrm{L},i} - P_{\mathrm{L}}$ and $P_{\mathrm{L},i} \approx P_{\mathrm{c}}$ which is similar results from Fornasiero et al. and Wheeler and Stroock (Fornasiero et al., 2008; Wheeler & Stroock, 2008).

2.4. Hydraulic capacitance until cavitation

The volume change of the synthetic tree until cavitation can be expressed by Equation 2.2 as follows: $\Delta V_{\mathrm{c}}/V_0 = C(P_{\mathrm{c}} - P_0)/V_0$. Here $\Delta \mathrm{V_c}$ is the volume

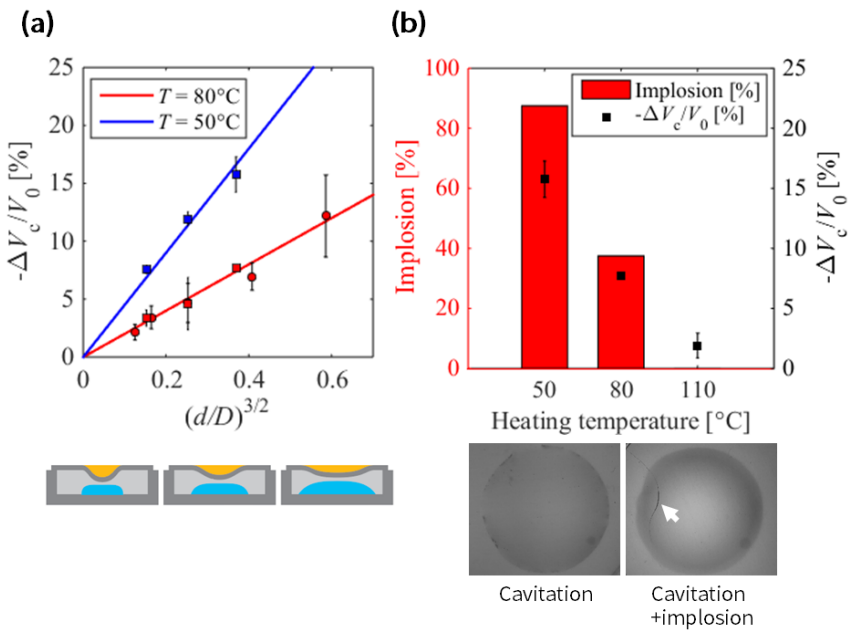

Figure 2.7. (a) Normalized volume loss until cavitation follows $(d/D)^{3/2}$. The volume change until cavitation increased with lower temperatures because it decreased the cavitation pressure. (b) Implosion rate of the synthetic trees increased in low heating temperature because of high pressure difference. $d = 20$ mm, $H = 2$ mm (•) and $d = 10$ mm, $H = 1.4$ mm (▪)

change of the synthetic tree until cavitation, V_0 is the initial volume of the deformable part, $(\pi/4)\,D^2H$, and P_c is the cavitation pressure. Our experiment confirmed that $-\Delta V_c/V_0$ was proportional to $(d/D)^{\alpha}$ (Figure 2.7a). Also, the larger the bending stiffness, K, of the membrane will lower the hydraulic capacitance. Thus, the capacitance of the artificial tree is expressed as:

$$C \sim \frac{V_0}{K}\left(\frac{d}{D}\right)^{\alpha} \tag{2.5}$$

Empirically, α was $3/2$.

2.5. Effect of temperature on cavitation and implosion

Assuming that cavitation happens as the nano-bubble hanging on PDMS cannot withstand the pressure difference, the cavitation pressure P_c is scaled to γ/r. γ is the surface tension coefficient of water and r is the pore size of PDMS. Since the surface tension coefficient, on the other hand, is a function of temperature, the cavitation pressure is affected by temperature (Vargaftik, Volkov, & Voljak, 1983) (Table 2.2).

Table 2.2. Surface tension coefficient of water in different temperature

Temperature (°C)	50	80	110
Surface tension coefficient (10^{-3} N/m)	67.94	62.67	56.96

In the experiment, cavitation happened in more volume changes in lower

heating temperatures. Because cavitation is delayed, the pressure difference across the membrane is increased in lower temperatures. Because the bending stress on the membrane is proportional to the pressure difference, $P_0 - P_L$ (Young, Budynas, & Sadegh, 2002), and it may make a fracture on the membrane. In experiments, a higher rate of fracture was observed in lower heating temperatures (Figure 2.7b).

2.6. Fabrication of synthetic tree with channels

The synthetic tree with ten channels was devised to observe the growth of the cavitation bubble (Figure 2.8). A double molding technique was used to fabricate the engraved hydrogel (Figure 2.9). This method was to mass-produce a secondary mold to protect the primary mold. First, the primary mold was fabricated by spin coating SU-8 on a silicon wafer. The thickness of the coated SU-8 was controlled to 50 micrometers. After UV light irradiation (385 nm), the mold was developed. Since SU-8 was cured when

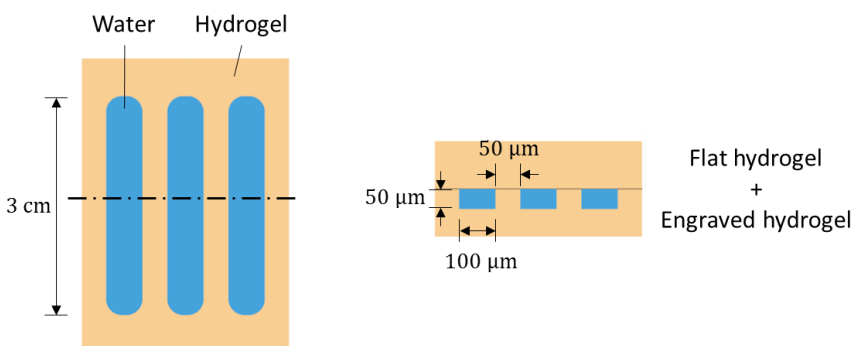

Figure 2.8. Schematic images of the synthetic tree which are made by putting together flat and engraved hydrogel sheets. It contains ten aligned bulk cavity filled with water.

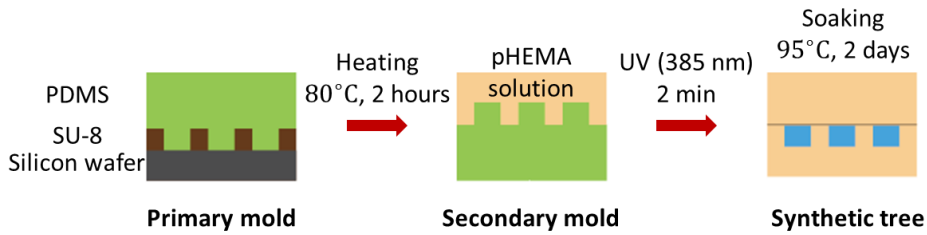

Figure 2.9. A double molding technique was used to fabricate the engraved hydrogel. The pre-cured engraved and flat hydrogel was put together and irradiated UV light (385 nm) for an extra 30 seconds to fully polymerize. Then, the hydrogel was soaked in 95°C water for two days to fill water and to remove chemical residues.

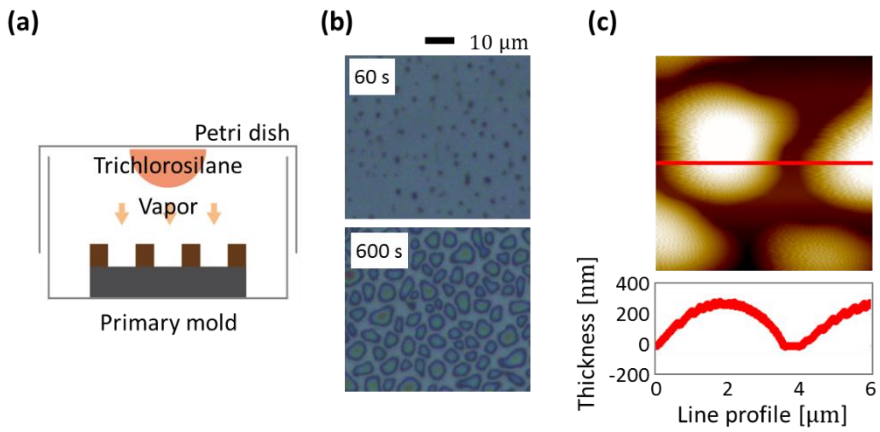

Figure 2.10. (a) Schematic image of physical vapor deposition (PVD) of trichlorosilane on the primary mold. (b) Optical microscopy image of bumps generation after PVD for 60 s and 600 s. (c) Atomic force microscopy scanning image of bumps after PVD for 600 s.

UV light had been irradiated, the part that does not receive UV light is removed during the development process. Based on this, the primary mold was obtained. Next, PDMS was applied and a secondary mold was formed by polymerization at a temperature of 80°C for two hours.

At this time, if the bonding strength between the PDMS and the primary mold is large, the primary mold may be broken during separation. To solve this problem, (tridecafluoro-1, 1, 2, 2 - tetrahydrooctyl) trichlorosilane was applied to the primary mold by the physical vapor deposition method (Figure 2.10a). Using it, trichlorosilane bumps of 4 micrometers width and 0.3 micrometers height can be produced on the primary mold (Figure 2.10bc). This lowers the bond between the mold and the PDMS, which makes it easier to separate.

Hydrogel solution was applied with 500 μm spacers on the PDMS secondary mold, covered with a slide glass, and applied UV light (385 nm) for about 2 minutes to partially polymerize. Then, a flat 500 μm hydrogel film is applied to the engraved hydrogel film. After that the UV light irradiation for 30 seconds completely polymerized the hydrogel.

In order to fill the empty space with water, it was soaked in water at about 95°C for two days. Meanwhile, the synthetic tree was fully saturated and the residue of polymerization had escaped from the hydrogel.

2.7. Observation of cavitation bubble

The synthetic tree is then placed in a cage with one-centimeter diameter holes at each end (Figure 2.11a). This is to control the evaporative area. Then it was

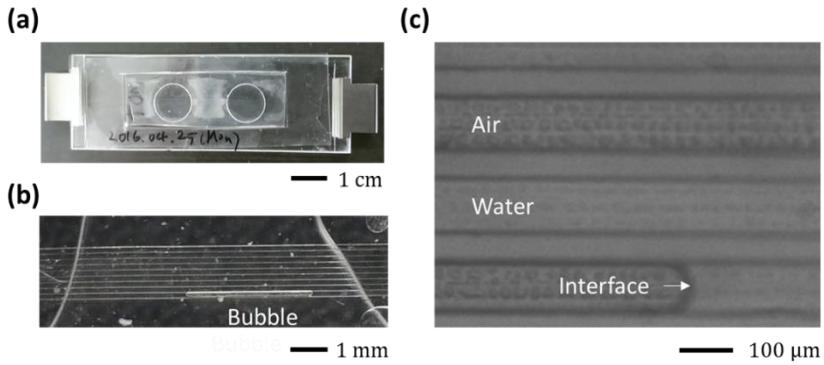

Figure 2.11. (a) Actual image of the synthetic in the cage. Two holes are to control the evaporating area. (b) The magnified image of the synthetic tree after cavitation (c) the optical microscope image of the synthetic tree after cavitation.

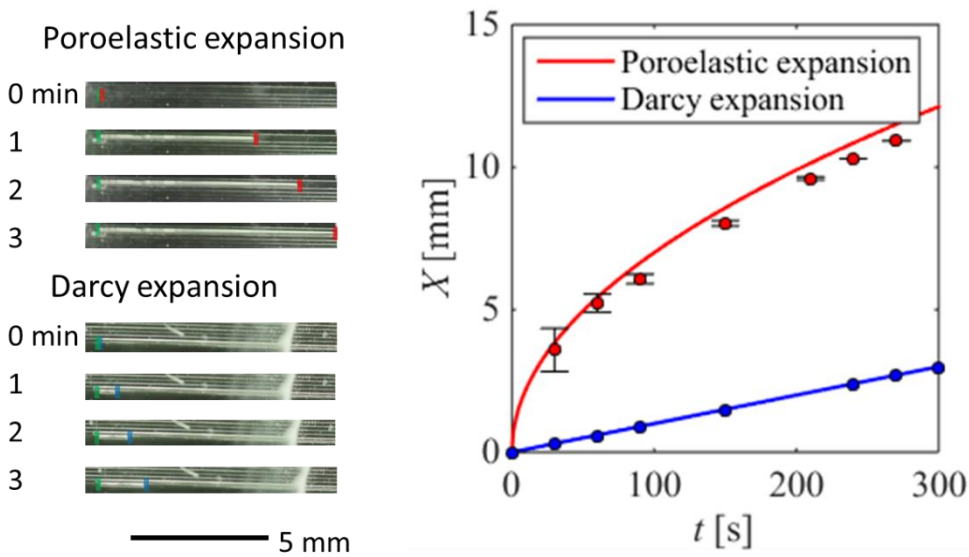

Figure 2.12. Two types of bubble expansion were observed. The speed of the bubble in the poroelastic expansion is fast but decelerated, and the speed of the bubble in Darcy expansion is slow but constant.

photographed every 30 seconds at atmospheric conditions of $20°C$ and 40% relative humidity (Figure 2.11b). The bubbles were formed within a few hours and the advancing of the bubble front with time was observed (Figure 2.11c). As a result, two expansion patterns were observed (Figure 2.12). When the initial expansion rate was high, the expansion rate was gradually decreased. When the rate was low, the speed was kept constant. The former case was named poroelastic expansion and the latter was named Darcy expansion.

2.9. Analysis of bubble expansion

To analyze the expansion of air bubbles inside the vessel element of the synthetic tree, it is necessary to be able to express the change of the pressure inside the porous media. The porous media is a structure in which fibers are tightly entangled. When observing a specific volume, δV, in porous media, the volume occupied by the fiber, $\phi\delta V$ does not change during the volume change of the specific volume, $\mathrm{d}/\mathrm{d}t\,(\delta V\phi) = 0$. The amount of liquid entering or exiting the surface of this volume segment when it swells or shrinks can be expressed as $\partial/\partial t\,(\delta V) = -\delta V\boldsymbol{\nabla}\cdot\boldsymbol{q}$ by the law of conservation of mass. $\boldsymbol{q}$ is the flux of water. Using these two equations, the pressure change over time of the volume segment can be expressed as follows:

$$\frac{\partial P}{\partial t} = -K\boldsymbol{\nabla}\cdot\boldsymbol{q} \tag{2.6}$$

K is the swelling modulus, $-\phi\,\partial P/\partial\phi$. The flow rate inside the porous media follows Darcy's law:

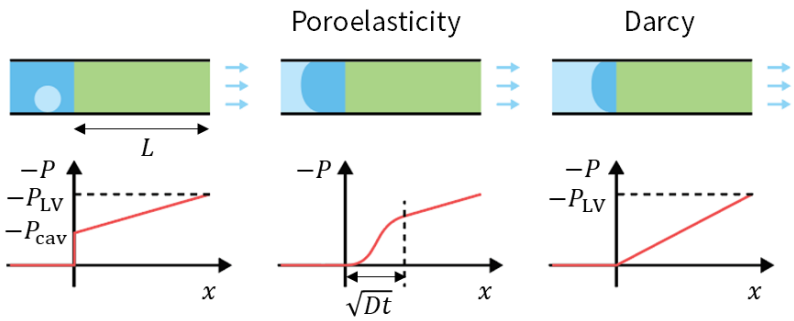

Figure 2.13. Pressure distribution of bulk liquid and porous media after cavitation. The poroelastic distance can be defined if $P_c \gg 0$.

$$\boldsymbol{q} = -\frac{k}{\mu}\boldsymbol{\nabla} P \tag{2.7}$$

μ is the viscosity of water. Permeability, k, is the function of fiber fraction, ϕ, but it can be regarded as constant in pHEMA hydrogel with a small swelling ratio. As a result, the pressure change inside the porous media follows the diffusion-like equation (Vincent et al., 2012):

$$\frac{\partial P}{\partial t} = D\nabla^2 P \tag{2.8}$$

D is the diffusion coefficient, kK/μ.

The meaning of the above equation is that when the pressure at a specific position in the porous media instantaneously changes in the difference of ΔP, the change poroelastically affects in distance of L_p in time t. By scaling approach, $\Delta P/t \sim D\Delta P/L_p^2$, the poroelastic distance, L_p, of the pressure difference, ΔP, follows (Figure 2.13):

$$L_{\mathrm{p}} \sim \sqrt{Dt} \tag{2.9}$$

During the evaporation of the synthetic tree, the pressure near the interface inside the porous media is $P_{\mathrm{L},i}$, and the pressure of bulk water is P_{L}. As the pressure of bulk water reaches cavitation pressure, P_{c}, cavitation happens and the pressure drastically increases into zero. Then, the pressure of porous media near the bulk water instantly increases in the difference of $\Delta P = P_{\mathrm{c}}$. By equation 2.7 and 2.9, poroelastic flowrate inside porous media follows:

$$q_{\mathrm{p}} \sim -\frac{k}{\mu}\frac{P_{\mathrm{c}}}{L_{\mathrm{p}}} \tag{2.10}$$

In contrast, If the bubble forms without negative pressure, $P_{\mathrm{c}} \approx 0$, the flow rate follows normal Darcy's law, equation 2.7:

$$q_{\mathrm{D}} \sim -\frac{k}{\mu}\frac{P_{\mathrm{L},i}}{L} \tag{2.11}$$

L is the thickness of the hydrogel.

Plotting the expansion of the bubbles with time shows that poroelastic expansion is applied for fast bubbles and Darcy expansion is applied for slow bubbles (Figure 2.14). That is, bubbles with a high expansion rate are formed with low cavitation pressure and bubbles with a low expansion rate are due to the cavitation pressure near zero.

According to the previous study, the diffusion coefficient, D, of

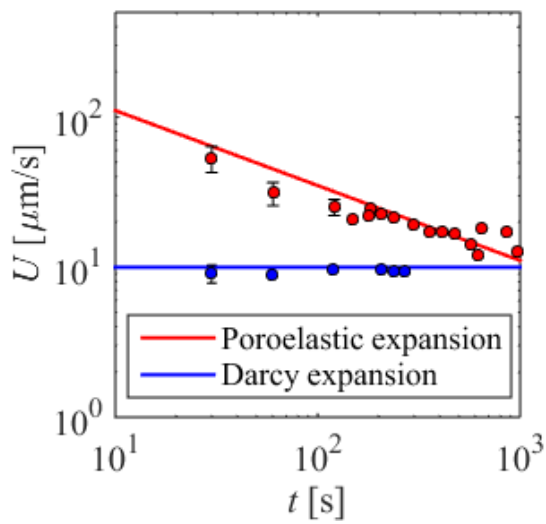

Figure 2.14. The bubble speed of poroelastic expansion follows $t^{-1/2}$ and that of Darcy expansion is constant.

pHEMA hydrogel is $10^{-11}\,\mathrm{m^2 s^{-1}}$ and k/μ is $10^{-19}\,\mathrm{m^2 Pa^{-1} s^{-1}}$ (Vincent et al., 2012). If the expansion rate of the bubble, u, satisfies the relation, $uA_\mathrm{v} = qA_\mathrm{p}$, where A_v is the cross-sectional area of a vessel element and A_p is evaporating area on porous media, according to the continuity equation, it can be seen that $P_\mathrm{c}, P_\mathrm{LV} \sim -10$ MPa, which is well agreed with previous studies (Fornasiero et al., 2008; Vincent et al., 2012; Wheeler & Stroock, 2008).

2.10. Discussion and conclusion

In this chapter, the process of embolization was divided into the propagation of the bubble and the growing of the bubble. For this purpose, a synthetic tree was fabricated and the experiments were analyzed.

As for the propagation of the bubble, it was confirmed that the larger the volume of water in the artificial plant, the larger the volume change until cavitation. That is, the volume of water is an important factor for hydraulic capacitance. We also confirmed that heating temperature is an important factor in determining cavitation pressure. That is, the lower the temperature, the lower the cavitation pressure. As a result, cavitation was delayed, but some membranes were broken because of the pressure difference.

As for the growth of the bubble, cavitation bubbles in the synthetic tree expand according to the two laws of physics according to the cavitation pressure. First, if the cavitation pressure is close to zero, the growth rate is slow and constant, following Darcy's equation. When the cavitation pressure is low, the initial growth speed is very fast, but poroselastically decelerates with time, following poroelastic expansion.

In real plants, a bubble will expand its size with the poroelastic manner if pit membranes work normally. However, a bubble will be generated easily with Darcy manner if there are micro-fractures on the pit membranes or vessel wall. Thus, plants should avoid fractures and their anatomical traits should be correlated with temperature (Moles et al., 2014).

Chapter 3. Comparative analysis

3.1. Physiological and anatomical traits of plant stem

The plant stem simultaneously delivers water to leaves and cambium; as well as stores sugar; and mechanically supports against gravity, wind, and cavitation. Consequently, it has specialized its components: vessel or tracheid, parenchyma, and fiber (Figure 3.1). Because they share the confined volume, the traits of stems show trade-off relations according to their proportions (Figure 3.2).

In order to conduct water efficiently, plants should increase the conduit diameter. The conductivity is consistent with the Hagen-Poiseuille equation (Sperry, Hacke, & Pittermann, 2006). Plants with efficient conductivity have also high photosynthetic productivity (Brodribb, 2009) since they must exchange carbon dioxide with water vapor.

Denser wood is known to convey greater mechanical stability (A. L. Jacobsen, Ewers, Pratt, Paddock, & Davis, 2005), such as Young modulus, rupture stress, and resilience to dynamic breakage (Chave et al., 2009). Also fibers and thick-walled vessels found in high-density wood protect vessels from implosion when water shortage creates a large pressure difference (Hacke, Sperry, Pockman, Davis, & McCulloch, 2001).

Parenchyma cells in stems and branches are a great sink of photosynthetic compounds for metabolism, transporting signals, and osmoregulation (Hartmann & Trumbore, 2016). The mean tangential fraction of parenchyma cells is 25% in angiosperms and only 8% in gymnosperms.

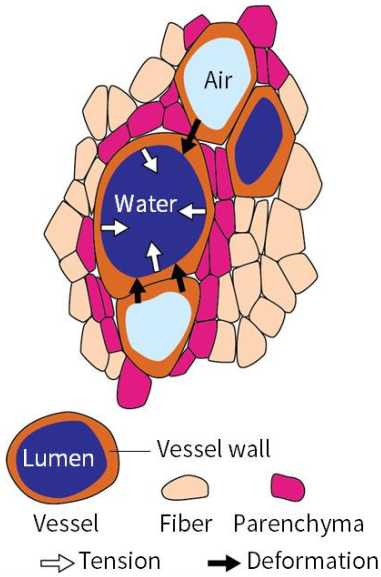

Figure 3.1. Cross section image of a plant stem. The physiological traits of plants stem results from the fraction of vessel, fiber, and parenchyma.

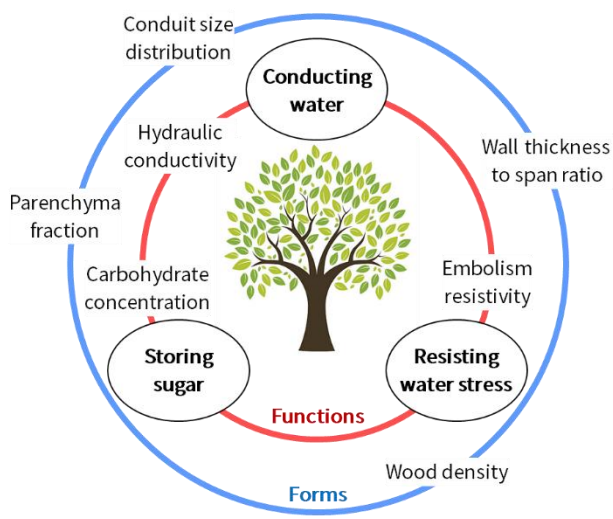

Figure 3.2. Three major functions of the plant stem and their trade-off relationship. Because anatomical traits follow physiological traits, we can indirectly measure the functions.

These percentage also have a correlation with nonstructural carbohydrate concentration (Johnson, McCulloh, Woodruff, & Meinzer, 2012). Species that experience drought are hypothesized to show high levels of parenchyma cells because of potential correlations of parenchyma cell fraction with drought resistance mechanisms such as refilling of embolised vessels (Brodersen & McElrone, 2013)

In this study, we will determine what anatomical relationship determines the embolism resistance of plant stems.

3.2. Definition of parameters

The hydraulic conductivity of plant stem and its mortality is highly related. Regardless of the species, they suddenly died when they lost 90% of conductivity by cavitation (Barigah et al., 2013). We selected the pressure, P_{50}, as an indicator of embolism resistance of plant stem, which is the pressure that causes cavitation to form so that the hydraulic conductivity of the stem is halved. The lower the P_{50}, the stronger the embolism resistance. Choat et al. found that plants with higher embolism resistance are living in drier climates (B. Choat et al., 2012).

Three parameters were selected to represent the anatomical characteristics of plant stems: wood fraction, η_{w}, parenchyma fraction, η_{p}, and lumen fraction, η_{l}. Wood fraction is the ratio of the cell wall to sapwood volume. This can be obtained by first measuring wood density and dividing it by the volume of cellulose $1.5\ \mathrm{g/cm^3}$ (Chave et al., 2009). There is a high correlation with wood fraction and the proportion of fiber (Martinez-Cabrera, Jones, Espino, & Schenk, 2009; Ziemińska, Butler, Gleason, Wright, &

Westoby, 2013). Next, parenchyma fraction is the ratio of parenchyma cells in the volume of sapwood. This can be obtained by measuring the proportion of parenchyma cells in the cross-section of the stem. Plants which live in tropical climates have more proportion of parenchyma cells than plants living in temperate climates (Morris et al., 2016). Finally, this study defined the lumen ratio as an important index. This is the ratio of the space filled with water or air in the sapwood and can be expressed as the subtraction of the volume of the cell wall and parenchyma cells in the total volume. In other words, the lumen ratio is $1 - \eta_{\mathrm{w}} - \eta_{\mathrm{p}}$.

3.3. Comparative analysis of plant stem

We adopted the database of the wood fraction (Chave et al., 2009), parenchyma fraction (Morris et al., 2016), embolism resistivity (B. Choat et al., 2012), and other literature (Fu & Meinzer, 2018; A. L. Jacobsen et al., 2005; Martinez-Cabrera et al., 2009; Pausas et al., 2016; Savi et al., 2018; ZHU, SONG, LI, & YE, 2013; Ziemińska et al., 2013; Zieminska, Westoby, & Wright, 2015). Totally, 538 species of angiosperms and 84 species of gymnosperms were collected (Table A.1 and A.2). Even though the way of reproduction and the shape of leaves is dramatically different between the two types of trees; however, they show the continuum hydraulic strategy at the whole plant level (Johnson et al., 2012).

There was no correlation between the wood fraction and parenchyma fraction (Figure 3.3a). However, it was supported that angiosperms had a higher percentage of parenchyma cells than gymnosperms. It is because gymnosperms have only radial parenchyma cells; whereas, angiosperms have

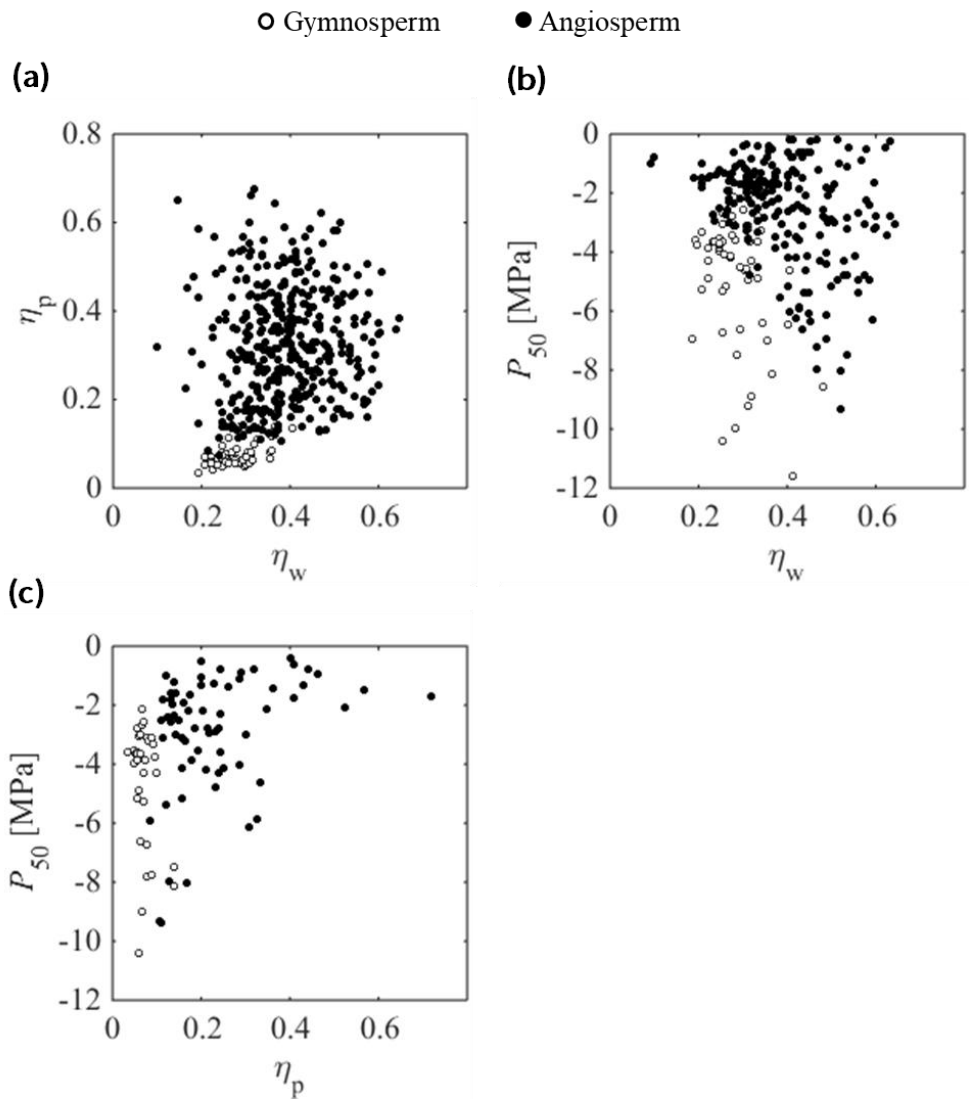

Figure 3.3. (a) The relation between wood fraction, η_w, and parenchyma fraction, η_p. (b) The relation between wood fraction, η_w, and embolism resistivity, P_{50}. (c) The relation between parenchyma fraction, η_p, and embolism resistivity, P_{50}.

axial and radial parenchyma cells (Spicer, 2014). In addition, it was verified that it is necessary to have a low parenchyma fraction and high wood fraction in order to have a high P_{50} (Figure 3.3bc). The results are well agreed with literature that high embolism resistivity demands high wood density not to collapse their conduits (Hacke et al., 2001; A. L. Jacobsen et al., 2005; Anna L Jacobsen, Pratt, Ewers, & Davis, 2007; Pratt, Jacobsen, Ewers, & Davis, 2007; Savi et al., 2018). Also, there is a trade-off relation between the proportion of the fibers and parenchyma cells (Martinez-Cabrera et al., 2009). Finally, plotting using P_{50} and lumen ratio showed that two boundaries were formed to have high embolism resistance (Figure 3.4). 64 species of angiosperms and 30 species of gymnosperms had enough information to be plotted.

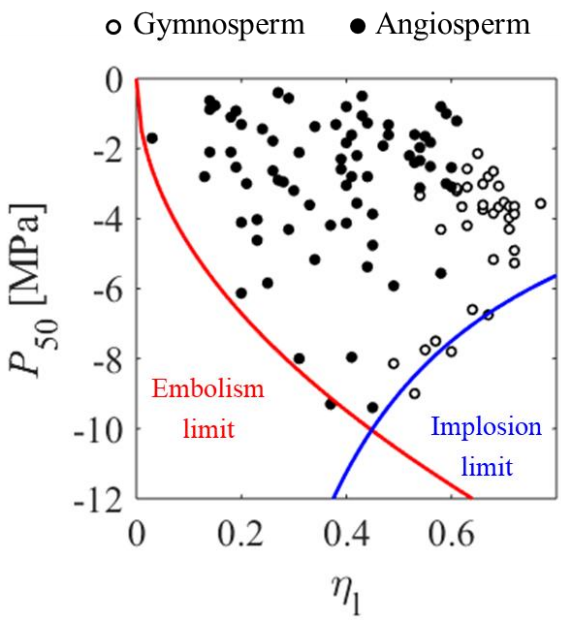

Figure 3.4. The relation between lumen ratio, η_l, and embolism resistivity, P_{50}. It shows two boundaries which limit the variety of lumen ratio to get high embolism resistivity.

3.4. Embolism limit

It can be seen from Equation 2. 2 and 2. 4 that cavitation time follows if the magnitude of interfacial pressure, $|P_{\mathrm{L},i}|$, is much larger than cavitation pressure, $|P_{\mathrm{c}}|$:

$$t_{\mathrm{c}} \sim RC\,\frac{P_{\mathrm{c}}}{P_{\mathrm{L},i}} \tag{3.1}$$

Our experimental data in Chapter 2 shows the relationship between the hydraulic capacitance, C, and structural parameter (d/D) as equation 2.5. Thus, equation 3.1 can be expressed as $t_{\mathrm{c}} \sim (RV_0/K)(P_{\mathrm{c}}/P_{\mathrm{LV}})(d/D)^{\alpha}$. Here, $(d/D)^2$ can be defined as the lumen ratio, and P_{LV} can be replaced by P_{50}, which is applying pressure during the measurement of cavitation resistivity. On the other hand, the plant vascular system can be sustainable if cavitation time is longer than the time needed for the plant to repair, t_{r}: $t_{\mathrm{c}} > t_{\mathrm{r}}$. Therefore, the lumen ratio of a plant has the following relationship:

$$\eta_{\mathrm{l}} > \left(t_r \left(\frac{K}{RV_0}\right)\left(\frac{P_{50}}{P_{\mathrm{c}}}\right)\right)^{2/\alpha} = \eta_{\mathrm{l}}^{\mathrm{c}} \tag{3.2}$$

In Figure 3.4, the minimum fraction of the lumen is expressed as the embolism limit (red line), which is $P_{50} = A(\eta_{\mathrm{l}}^{c})^{\alpha/2}$. Here α is 1 and the pre-factor is 15. That is, if the lumen ratio is too small, the plant cannot survive because cavitation happens too frequently.

3.5. Implosion limit

The vessel must be reinforced with lignin and a thick secondary layer to resist collapse by internal negative pressure (Hacke et al., 2001). The bending stress on the wall of a plant vessel wall is as follows (Young et al., 2002):

$$\sigma = (P_0 - P_{\mathrm{L}})\left(\frac{b}{t}\right)^2 \tag{3.3}$$

Where b is the lumen diameter and t is the vessel wall thickness. Therefore, wider conduits must grow thicker walls and (b/t) can be expressed as $(\eta_{\mathrm{l}}/\eta_{\mathrm{w}})$. When the bending stress on the wall is larger than the critical stress σ_{b}, implosion occurs. Then, pit membranes on the vessel wall cannot work properly because of micro-fracture by the vessel implosion (Venturas, Sperry, & Hacke, 2017). Thus, lumen fraction cannot exceed the critical value as follows:

$$\eta_{\mathrm{l}} < \left(\frac{\sigma_{\mathrm{b}}}{P_{50}}\right)^{0.5} \eta_{\mathrm{w}} = \eta_{\mathrm{l}}^{\mathrm{b}} \tag{3.4}$$

In Figure 3.4, the maximum fraction of the lumen is expressed as the implosion limit (blue line), which is $P_{50} = B\left(\eta_{\mathrm{l}}^{b}\right)^{\beta}$. Here β is -1, and the pre-factor is -4.5. That is, if the lumen ratio is too large, the plant cannot survive because their conduits collapse easily. Researchers found that implosion of the vessel wall happens in lignin deficient mutant which has lower critical stress (Kitin et al., 2010; Piquemal et al., 1998).

3.6. Discussion and conclusion

In this chapter, we plotted biological data on the lumen fraction and P_{50} plane and analyzed how the boundary of the regime is expressed. As a result, the regime is restricted by two different limits. First, plants can take a strategy to increase embolism resistivity by increasing hydraulic capacitance. Plants can increase the lumen ratio as in Chapter 2 to increase the hydraulic capacitance. However, if the lumen ratio is too large, it may be vulnerable to implosion. Therefore, unless cavitation is formed, reducing the lumen ratio may increase the embolism resistivity.

In the embolism limit, pre-factor, A, is proportional to cavitation pressure, P_c. This correlation makes sense because the cavitation pressure is determined by the properties of the pit membrane in order to protect from air-seeding. Thus, embolism resistivity will increase if a stem has thick and dense pit membranes. In the implosion limit, on the other hand, the pre-factor, B, is proportional to wood fraction, η_w. This correlation also holds to avoid suffering from vessel implosion (Hacke et al., 2001; A. L. Jacobsen et al., 2005; Anna L Jacobsen et al., 2007; Pratt et al., 2007; Savi et al., 2018). Thus,

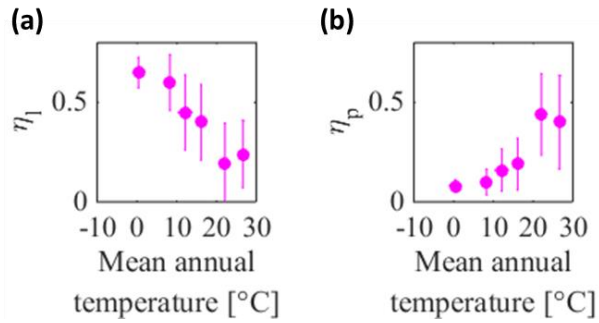

Figure 3.5. (a) The relation between mean annual temperature and lumen fraction, η_l. (b) The relation between mean annual temperature and parenchyma fraction, η_p.

embolism resistivity also depends on the size of pit membrane pores and the strength of vessels to resist collapse (Anna L Jacobsen et al., 2007).

Interestingly, the strategy to increase cavitation resistance depends on the different species. While angiosperms take a strategy to increase the lumen ratio, gymnosperms take a strategy to reduce the lumen ratio. This can be attributed to differences in habitat conditions (Figure 3.5a). Angiosperms live in a high-temperature environment whereas conifers live in a low-temperature environment. As we have seen in Chapter 2, at high temperatures, bubbles occur more easily because the cavitation pressure increases. Therefore, angiosperms are likely to have chosen the structure according to a strategy to suppress cavitation. Indeed, in the case of angiosperms, the parenchyma fraction in the stem is much higher than that of gymnosperms (Figure 3.5b). Among two genera of gymnosperm (*Podocarpus* and *Dacrydium*), in addition, trees living in the tropical/subtropical mountain have higher parenchyma fraction than those living in cooler, more temperate region (Braun, 1984). Parenchyma cells are known to contribute to embolism repair (Nardini, Lo Gullo, & Salleo, 2011; Zwieniecki & Holbrook, 2009). On the other hand, gymnosperms are likely to have selected their strategies to cope with implosion rather than embolism because they live in a low-temperature environment.

Chapter 4. Concluding remarks

4.1. Conclusions

The study began with a question about how plants could survive in a dry environment. If water is not supplied properly, bubbles form inside, which is fatal to plants. We confirmed the mechanism of the propagation and the growth of the bubble by performing experiments in the synthetic tree model system. Next, based on the experimental results, how the anatomical features of plant stem contribute to cavitation resistance is analyzed.

In Chapter 2, the process of embolization was divided into the propagation of the bubble and the growing of the bubble. For this purpose, a synthetic tree was fabricated and the experiments were analyzed.

As for the propagation of the bubble, it was confirmed that the larger the volume of water in the artificial plant, the larger the volume change until cavitation. That is, the volume of water is an important factor for hydraulic capacitance. We also confirmed that heating temperature is an important factor in determining cavitation pressure. That is, the lower the temperature, the lower the cavitation pressure. As a result, cavitation was delayed, but some membranes were broken because of the pressure difference.

As for the growth of the bubble, cavitation bubbles in the synthetic tree expand according to the two laws of physics according to the cavitation pressure. First, if the cavitation pressure is close to zero, the growth rate is slow and constant, following Darcy's equation. When the cavitation pressure is low, the initial growth speed is very fast, but poroselastically decelerates

with time.

Actual plants are likely to postpone the propagation of the bubble to delay the process of embolization. This is because the xylem of the plant is not only compartmented but also has a pit membrane designed between the vessel elements. If the pit membranes work properly, the bubbles will undergo poroelastic expansion; however, the bubbles will form easily by Darcy expansion if there is a rupture in the membrane or vessel wall.

In Chapter 3, we plotted biological data on the lumen fraction and P_{50} plane and analyzed how the boundary of the regime is expressed. As a result, the regime is restricted by two different limits. First, plants can follow a strategy to increase embolism resistivity by increasing hydraulic capacitance. Plants can increase the lumen ratio as in Chapter 2 to increase the hydraulic capacitance. However, if the lumen ratio is too large, it may be vulnerable to implosion. Therefore, unless cavitation is formed, reducing the lumen ratio may increase the embolism resistivity.

Interestingly, the strategy to increase cavitation resistance depends on the different species. While angiosperms take a strategy to increase the lumen ratio, gymnosperms take a strategy to reduce the lumen ratio. This can be attributed to differences in habitat conditions (Figure 3.5a). Angiosperms live in a high-temperature environment whereas conifers live in a low-temperature environment. As we have seen in Chapter 2, at high temperatures, bubbles occur more easily because the cavitation pressure increases. Therefore, angiosperms are likely to have chosen the structure according to a strategy to suppress cavitation. Indeed, in the case of angiosperms, the parenchyma fraction in the stem is much higher than that of gymnosperms (Figure 3.5b). Parenchyma cells are known to contribute to embolism repair (Nardini et al.,

2011). On the other hand, gymnosperms are likely to have selected their strategies to cope with implosion rather than embolism because they live in a low-temperature environment.

4.2. Future works

Angiosperms living in arid climates have a high rate of axial parenchyma cells around their xylem, which have non-structured carbohydrates (NSC) in their cytoplasm. NSC will be used in the metabolic process (Hartmann & Trumbore, 2016). Thus, parenchyma cells are Maxwell's demon of embolism repair (Zwieniecki & Holbrook, 2009). This research proposes to understand how physical supports from water potential gradient and material properties of the xylem system can repair the dysfunction.

Embolism-repair-like condensation was observed in synthetic tree experiments (Figure 4.1). It is hypothesized that a steep potential gradient

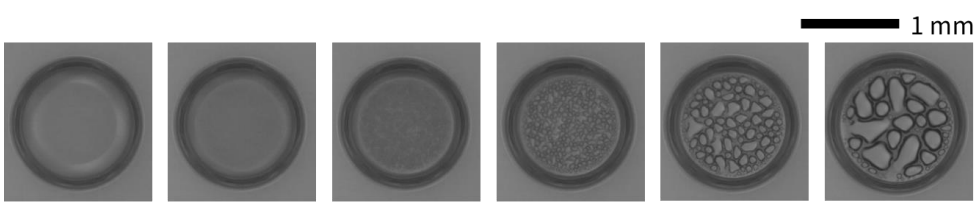

Figure 4.1. Change of embolism-repair-like condensation inside the cavity of a synthetic tree

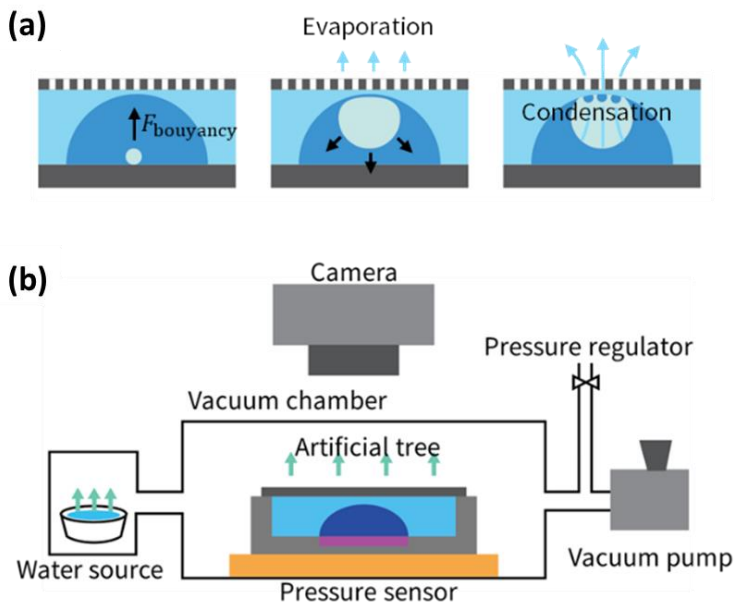

Figure 4.2. (a) The hypothesis of embolism-repair-like condensation. (b) Experimental apparatus.

generates condensing droplets inside the cavity of the synthetic tree (Fig. 4.2a). To verify the hypothesis, we will control the humidity of the atmosphere by a water source, a vacuum pump, and a pressure regulator. Then, we will measure the evaporative mass loss by using a pressure sensor beneath the artificial tree (Fig. 4.2b). Finally, we will get high quality sequential pictures of embolism-repair-like condensation after cavitation. I expect that the faster droplets will generate in the drier atmosphere. Thus, some portion of water in embolism repair will be generated passively by means of physical rules.

We can indirectly evaluate embolism repair by measuring anatomical traits of plants stems. We can improve Figure 3.4 by measuring wood density, parenchyma ratio, and embolism resistivity of missing species. I propose that exploring Fynbos will further enlighten the unknown mechanism of embolism repair because of the variety of species in very small areas. Fynbos is naturally growing vegetation found on the mountains and coastal plains of the southwestern tip of South Africa. It occupies a relatively small area of land. There are over 7,000 species across a 41,000 km^2 of land.

Appendix A

Table. A.1. Biological data for 539 species of angiosperm collected from literature study.[1]

Species	P_{50} [MPa]	η_w	η_p	MAT [°C]	Ref
Acacia dealbata		0.36	0.24		[5]
Acacia flavescens		0.51	0.18		[4]
Acacia greggii	-0.88	0.57	0.29	16.0	[1, 3, 7]
Acacia mangium		0.27	0.30		[4]
Acacia melanoxylon		0.34	0.26		[5]
*A*cacia obliquinervia		0.37	0.17		[5]
Acacia tenuifolia		0.33	0.46		[2, 3]
Acer campestre	-2.00	0.35		8.4	[1, 2]
Acer campestre	-4.19	0.40		8.4	[6]
Acer monspessulanum	-4.78	0.53		10.9	[6]
Acer negundo	-1.34	0.28		16.4	[1, 2]
Acer pictum		0.42	0.18		[2, 3]
Acer platanoides	-1.80	0.34		8.4	[1, 2]
Acer pseudoplatanus	-1.60	0.34	0.13	11.7	[1-3]
Acer rubrum	-1.97	0.33	0.13	15.0	[1-3]
Acer saccharinum	-1.00	0.29	0.12	8.2	[8]
Acer saccharum	-3.87	0.37	0.18	7.2	[1-3]
Acosmium nitens		0.49	0.44		[2, 3]
Adansonia za	-1.70	0.253333	0.72	24.3	[1, 3]
Adenostoma fasciculatum	-8.23	0.59	0.47	14.6	[1, 3, 10]
Afzelia bipindensis		0.46	0.37		[2, 3]
Afzelia quanzensis		0.46	0.33		[2, 3]
Albizia saman		0.33	0.35		[2, 3]
Albizia zygia		0.34	0.56		[2, 3]

[1] P_{50} is the pressure that causes cavitation to form so that the hydraulic conductivity of the stem is halved; η_w is wood fraction of sapwood, η_p is parenchyma fraction of sapwood; and MAT is mean annual temperature of the habitat.

Aldina latifolia		0.50	0.58		[2, 3]
Aleurites moluccana	-2.17	0.27		21.7	[1, 2]
Allocasuarina monilifera		0.39	0.33		[4]
Allocasuarina torulosa		0.41	0.21		[4]
Alnus glutinosa	-2.20	0.29		9.0	[1, 2]
Alnus incana	-1.70	0.29		9.6	[1, 2]
Alnus rubra	-2.54	0.25	0.15	10.4	[1-3]
Alphitonia excelsa	-5.56	0.25	0.17		[1, 4]
Alstonia congensis		0.20	0.28		[2, 3]
Amanoa oblongifolia		0.55	0.48		[2, 3]
Amphimas pterocarpoides		0.31	0.60		[2, 3]
Amphirrhox longifolia		0.47	0.55		[2, 3]
Amyxa pluricornis	-0.63	0.43		27.1	[1, 2]
Anacardium excelsum	-1.56	0.27		26.9	[1, 2]
Anacardium occidentale		0.28	0.36		[2, 3]
Andira inermis		0.42	0.49		[2, 3]
Anisoptera costata		0.33	0.32		[2, 3]
Annona glabra	-3.30	0.33		26.3	[1, 2]
Antiaris toxicaria		0.23	0.34		[2, 3]
Antirhea tenuiflora		0.38	0.41		[5]
Antrocaryon klaineanum		0.35	0.17		[2, 3]
Aotus ericoides		0.45	0.33		[4]
Arbutus unedo	-3.09	0.43		10.9	[1, 2]
Argyrodendron peralatum		0.39	0.59		[5]
Artemisia californica	-1.83	0.49	0.11	15.2	[1, 3, 9]
Aspidosperma cylindrocarpon	-2.90	0.50	0.23		[8]
Aspidosperma polyneuron		0.51	0.18		[2, 3]
Aspidosperma quebracho-blanco		0.43	0.28		[2, 3]
Aspidosperma rigidum		0.31	0.34		[2, 3]
Astronium fraxinifolium		0.57	0.20		[2, 3]
Aucoumea klaineana		0.25	0.14		[2, 3]
Austromuellera trinervia		0.31	0.52		[5]
Autranella congolensis		0.37	0.42		[2, 3]
Avicennia officinalis		0.39	0.37		[2, 3]
Baikiaea plurijuga		0.51	0.38		[2, 3]

Baillonella toxisperma		0.49	0.44		[2, 3]
Balizia elegans		0.33	0.27		[2, 3]
Banksia marginata		0.35	0.27		[4]
Barringtonia racemosa	-1.36	0.31		20.9	[1, 2]
Batocarpus amazonicus		0.43	0.38		[2, 3]
Berlinia bracteosa		0.40	0.38		[2, 3]
Betula alleghaniensis		0.37	0.13		[2, 3]
Betula occidentalis	-1.52	0.34		9.6	[1, 7]
Betula papyrifera	-2.34	0.32	0.14	-4.1	[1-3]
Betula pendula	-2.40	0.35	0.12	8.3	[1-3]
Bischofia javanica	-1.27	0.38		21.7	[1, 2]
Blepharocalyx salicifolius	-1.72	0.51		21	[1, 2]
Bossiaea cinerea		0.55	0.29		[4]
Brachystegia cynometroides		0.38	0.33		[2, 3]
Brachystegia spiciformis		0.40	0.42		[2, 3]
Brombya platynema		0.38	0.37		[5]
Bruguiera gymnorhiza		0.56	0.26		[2, 3]
Burkea africana		0.34	0.44		[2, 3]
Bursera simaruba	-1.00	0.21		26.3	[1, 2]
Buxus sempervirens	-8.00	0.52	0.17	13.1	[1-3]
Caesalpinia echinata		0.57	0.16		[2, 3]
Calycanthus floridus	-2.11	0.34	0.35	10.5	[1, 3, 9]
Calycophyllum candidissimum	-2.87	0.49		26.0	[1, 2]
Campsiandra comosa		0.54	0.44		[2, 3]
Canarium caudatum	-1.47	0.22		27.3	[1, 2]
Canarium schweinfurtii		0.19	0.15		[2, 3]
Canella winterana	-0.23	0.63		23.4	[1, 2]
Carapa guianensis	-0.80	0.35	0.25	28.3	[1-3]
Cardwellia sublimis		0.31	0.66		[5]
Cariniana estrellensis		0.52	0.44		[2, 3]
Cariniana pyriformis		0.39	0.34		[2, 3]
Carpinus betulus	-4.31	0.47	0.24	8.3	[1, 3, 6]
Carpinus orientalis	-4.31	0.53		13.6	[6]
Carya glabra	-2.10	0.44		15.0	[1, 2]
Carya ovata	-0.56	0.43	0.28		[2, 3, 12]

Caryocar brasiliense	-1.48	0.43		21	[1, 2]
Casearia dallachii		0.34	0.38		[5]
Casearia javitensis		0.49	0.24		[2, 3]
Cassipourea guianensis		0.55	0.21	26.3	[2, 3]
Castanea dentata		0.27	0.13		[2, 3]
Castanopsis echinocarpa		0.41	0.56		[2, 3]
Castanopsis indica		0.38	0.52		[2, 3]
Castanospermum australe		0.29	0.54		[5]
Ceanothus crassifolius	-9.40	0.440586	0.11	16.6	[1, 3]
Ceanothus cuneatus	-7.96	0.47	0.13	16.5	[1-3]
Ceanothus leucodermis	-3.56	0.385333	0.19	16.5	[1, 3]
Ceanothus megacarpus	-9.30	0.52	0.11	14.4	[1, 3, 10]
Ceanothus oliganthus	-4.13	0.45	0.16	14.6	[1-3]
Ceanothus spinosus	-5.38	0.44	0.12	14.4	[1, 3, 10]
Cecropia concolor	-0.80	0.10	0.32		[8]
Cedrela fissilis		0.37	0.64		[2, 3]
Cedrela odorata		0.29	0.38		[2, 3]
Ceiba aesculifolia		0.32	0.68		[2, 3]
Ceiba pentandra		0.17	0.45		[2, 3]
Celtis laevigata		0.31	0.30		[2, 3]
Celtis occidentalis		0.33	0.22		[2, 3]
Cercis canadensis	-2.52	0.43		15	[1, 2]
Cercis siliquastrum	-1.80	0.40		14.2	[1, 2]
Cercocarpus betuloides	-7.46	0.53			[1, 2]
Cercocarpus ledifolius	-4.96	0.51		6.6	[1, 7]
Chaetocarpus schomburgkianus		0.53	0.32		[2, 3]
Chionanthus ramiflorus		0.37	0.26		[4]
Chlorocardium rodiei		0.59	0.22		[2, 3]
Chrysophyllum cainito	-2.10	0.49		26.9	[1, 2]
Chukrasia tabularis		0.34	0.27		[2, 3]
Cinnamomum camphora	-1.24	0.31		20.9	[1, 2]
Cleistanthus myrianthus		0.36	0.35		[5]
Coffea arabica	-2.54	0.41		23.4	[1, 2]
Colophospermum mopane		0.60	0.35		[2, 3]
Copaifera salikounda		0.48	0.32		[2, 3]

Coprosma hirtella		0.40	0.39		[5]
Cordia alliodora	-1.78	0.33	0.41	28.2	[1-3]
Cordia collococa	-2.34	0.28			[1, 7]
Cordia dentata	-3.60	0.31			[1, 2]
Cordia lasiocalyx	-2.57	0.26		26.3	[1, 2]
Cordia millenii		0.34	0.33		[2, 3]
Cornus florida	-5.84	0.43	0.33	15.0	[1-3]
Cornus sanguinea	-6.37	0.45		10.9	[1, 2]
Corylus avellana	-2.86	0.35		8.4	[6]
Corymbia citridora		0.42	0.18		[5]
Corymbia clarksoniana		0.37	0.12		[5]
Corymbia erythrophloia	-1.64	0.60		24.4	[1, 2]
Corymbia intermedia		0.43	0.21		[4]
Cotinus coggygria	-2.64	0.38			[6]
Cotylelobium burckii	-0.45	0.54		27.3	[1, 2]
Crataegus monogyna	-4.81	0.57		8.4	[6]
Crateva tapia		0.37	0.39		[2, 3]
Crescentia alata		0.47	0.45		[2, 3]
Cryptocarya grandis		0.38	0.36		[5]
Cryptocarya mackinnoniana		0.41	0.44		[5]
Cryptocarya murrayi		0.32	0.44		[5]
Cupania cinerea		0.33	0.41		[2, 3]
Cupania scrobiculata		0.34	0.17		[2, 3]
Curatella americana	-1.48	0.43	0.57	25.6	[1-3]
Dacryodes buettneri		0.33	0.18		[2, 3]
Dacryodes pubescens		0.37	0.13		[2, 3]
Dalbergia frutescens		0.52	0.22		[2, 3]
Dalbergia latifolia		0.53	0.30		[2, 3]
Dalbergia nigra		0.45	0.45		[2, 3]
Dalbergia retusa		0.59	0.30		[2, 3]
Daniellia ogea		0.29	0.21		[2, 3]
Davesia latifolia		0.43	0.32		[4]
Dendrobangia boliviana		0.41	0.37		[2, 3]
Dendropanax arboreus		0.27	0.19		[2, 3]
Detarium senegalense		0.47	0.37		[2, 3]

Dicorynia guianensis		0.41	0.38		[2, 3]
Didelotia africana		0.34	0.31		[2, 3]
Dillenia pentagyna		0.42	0.34		[2, 3]
Diospyros brachiata	-0.42	0.36			[1, 2]
Diospyros celebica		0.59	0.33		[2, 3]
Diospyros hermaphroditica	-0.60	0.40			[1, 2]
Diospyros mindanaensis	-0.79	0.43		27.1	[1, 2]
Diospyros virginiana	-0.63	0.45	0.41	17.1	[1-3]
Dipterocarpus alatus		0.37	0.29		[2, 3]
Dipterocarpus globosus	-0.18	0.47		27.1	[1, 2]
Dipterocarpus indicus		0.41	0.30		[2, 3]
Dipteryx oleifera		0.64	0.36		[2, 3]
Distemonanthus benthamianus		0.40	0.33		[2, 3]
Doryphora aromatica		0.36	0.24		[5]
Dracontomelon dao		0.34	0.26		[2, 3]
Drimys winteri	-2.30	0.27		12.2	[1, 2]
Dryobalanops aromatica	-0.26	0.45			[1, 2]
Dysoxylum alliaceum		0.29	0.49		[5]
Dysoxylum arborescens		0.35	0.44		[5]
Dysoxylum papuanum	-2.63	0.35	0.39		[5, 13]
Dysoxylum parasiticum		0.29	0.31		[5]
Dysoxylum pettigrewianum		0.31	0.43		[5]
Elaeocarpus angustifolius		0.27	0.30		[2, 3]
Elaeocarpus grandis	-3.05	0.30	0.30		[5, 13]
Encelia farinosa	-6.13	0.49	0.31	16.0	[1, 3, 9]
Endiandra leptodendron		0.38	0.36		[5]
Endiandra microneura		0.41	0.37		[5]
Entandrophragma angolense		0.34	0.36		[2, 3]
Entandrophragma candollei		0.40	0.43		[2, 3]
Entandrophragma cylindricum		0.38	0.38		[2, 3]
Entandrophragma utile		0.35	0.31		[2, 3]
Enterolobium cyclocarpum	-2.73	0.26		26.0	[1, 2]
Epacris impressa		0.47	0.36		[4]
Erisma calcaratum		0.45	0.41		[2, 3]
Erythrina stricta		0.15	0.65		[2, 3]

Erythrochiton fallax		0.30	0.39		[2, 3]
Erythrophleum suaveolens		0.39	0.46		[2, 3]
Eschweilera albiflora		0.57	0.51		[2, 3]
Eschweilera sagotiana		0.55	0.39		[2, 3]
Eucalyptus accedens	-3.20	0.60		17.7	[1, 2]
Eucalyptus amygdalina		0.40	0.16		[4]
Eucalyptus camaldulensis	-4.03	0.49	0.29	25.5	[8]
Eucalyptus capillosa	-3.08	0.64		17.1	[1, 2]
Eucalyptus diversicolor	-0.99	0.52		15.5	[1, 2]
Eucalyptus globulus	-1.10	0.54	0.29		[8]
Eucalyptus gomphocephala	-2.22	0.58		17.3	[1, 2]
Eucalyptus grandis	-1.31	0.42	0.20	21.8	[1-3]
Eucalyptus marginata	-1.24	0.47		17.7	[1, 2]
Eucalyptus pauciflora	-1.61	0.41	0.19		[5, 14]
Eucalyptus platyphylla		0.33	0.22		[4]
Eucalyptus tenuiramis		0.50	0.16		[4]
Eucalyptus tereticornis		0.55	0.28		[2, 3]
Eucalyptus urophylla		0.27	0.20		[2, 3]
Eucalyptus wandoo	-3.41	0.62		17.7	[1, 2]
Eugenia muelleri	-0.54	0.58			[1, 2]
Euonymus europaeus	-5.14	0.40		10.9	[1, 2]
Eupomatia laurina	-0.40	0.33	0.40	21.7	[1, 5]
Exocarpos strictus		0.40	0.36		[5]
Fagus sylvatica	-3.20	0.53	0.16	9.5	[1, 3, 6]
Ficus benjamina		0.28	0.47		[2, 3]
Ficus citrifolia	-1.60	0.27		26.3	[1, 2]
Ficus exasperata		0.23	0.57		[2, 3]
Ficus ingens		0.34	0.53		[2, 3]
Ficus insipida	-1.66	0.21		26.9	[1, 2]
Ficus mucuso		0.27	0.53		[2, 3]
Ficus thonningii		0.29	0.57		[2, 3]
Ficus variegata		0.27	0.36		[5]
Fraxinus americana	-1.92	0.37	0.16	10.0	[1-3]
Fraxinus excelsior	-2.80	0.37	0.19	9.1	[1-3]
Fraxinus latifolia		0.33	0.17		[2, 3]

Fraxinus nigra		0.30	0.19		[2, 3]
Fraxinus ornus	-3.48	0.42		14.7	[6]
Galbulimima baccata	-1.30	0.31			[1, 2]
Gastrolobium grandiflorum		0.47	0.26		[4]
Gilbertiodendron dewevrei		0.46	0.27		[2, 3]
Gillbeea whypallana		0.28	0.29		[5]
Gmelina arborea		0.23	0.36		[2, 3]
Gomphandra australiana		0.31	0.55		[5]
Gonystylus bancanus		0.34	0.18		[2, 3]
Gossweilerodendron balsamiferum		0.19	0.43		[2, 3]
Goupia glabra		0.47	0.36		[2, 3]
Grevillea glauca*		0.40	0.44		[5]
Grevillea parallela		0.40	0.52		[5]
Grevillea parallela		0.42	0.38		[4]
Guaiacum officinale		0.72	0.15		[2, 3]
Guarea cedrata		0.37	0.32		[2, 3]
Guarea guidonia		0.51	0.58	21	[2, 3]
Guarea thompsonii		0.37	0.42		[2, 3]
Guatteria schomburgkiana		0.40	0.39		[2, 3]
Guazuma ulmifolia		0.34	0.46		[2, 3]
Guettarda uruguensis		0.49	0.31		[2, 3]
Guibourtia arnoldiana		0.52	0.33		[2, 3]
Guibourtia ehie		0.52	0.31		[2, 3]
Guibourtia tessmannii		0.50	0.26		[2, 3]
Hakea lissosperma		0.36	0.30		[5]
Hakea microcarpa		0.41	0.41		[5]
Haplostichanthus ramiflorus		0.38	0.46		[5]
Harpullia rhyticarpa		0.41	0.31		[5]
Hebepetalum humiriifolium		0.57	0.20		[2, 3]
Heliocarpus americanus		0.18	0.48		[2, 3]
Heritiera simplicifolia		0.43	0.42		[2, 3]
Heritiera sumatrana	-1.69	0.35		27.1	[1, 2]
Hernandia albiflora		0.31	0.37		[5]
Hevea brasiliensis	-1.27	0.33	0.23	21.7	[1-3]

Hirtella triandra		0.53	0.50		[2, 3]
Hopea odorata		0.45	0.23		[2, 3]
Humiria balsamifera		0.44	0.26		[2, 3]
Humiriastrum cuspidatum		0.48	0.30		[2, 3]
Hura crepitans		0.25	0.25		[2, 3]
Hybanthus prunifolius	-2.60	0.45		26.3	[1, 2]
Hymenaea courbaril	-3.00	0.49	0.30	26.0	[1-3]
Hymenaea martiana	-2.80	0.60		21	[1, 2]
Hymenaea stigonocarpa	-3.17	0.60		21	[1, 2]
Idiospermum australiense	-0.62	0.43		24.7	[1, 2]
Ilex aquifolium	-6.60	0.43		10.9	[1, 2]
Inga edulis		0.51	0.47		[2, 3]
Inga semialata		0.40	0.32		[2, 3]
Inga umbellifera		0.48	0.43		[2, 3]
Intsia bijuga		0.50	0.26		[2, 3]
Isoberlinia doka		0.45	0.59		[2, 3]
Isonandra lanceolata	-0.48	0.62		27.3	[1, 2]
Ixora timorensis		0.35	0.31		[4]
Jacaranda mimosifolia	-2.10	0.34	0.53	22.0	[8]
Juglans cinerea		0.24	0.19		[2, 3]
Juglans nigra		0.34	0.15		[2, 3]
Juglans regia	-2.30	0.37	0.24	10.2	[1-3]
Julbernardia pellegriniana		0.43	0.23		[2, 3]
Kalmia latifolia		0.41	0.18		[2, 3]
Khaya ivorensis		0.28	0.27		[2, 3]
Laetia corymbulosa		0.44	0.39		[2, 3]
Laetia suaveolens		0.39	0.33		[2, 3]
Lagerstroemia microcarpa		0.33	0.32		[2, 3]
Laguncularia racemosa	-3.40	0.40		25	[1, 2]
Larrea tridentata	-2.8	0.63	0.24	18.3	[3, 7]
Lecythis poiteaui		0.52	0.42		[2, 3]
Leea indica		0.26	0.43		[5]
Leionema phylicifolium		0.41	0.20		[5]
Leptospermum scoparium		0.49	0.20		[4]
Leucopogon ericoides		0.45	0.31		[4]

Leucopogon ericoides		0.47	0.18		[4]
Licania membranacea		0.59	0.27		[2, 3]
Licania parviflora		0.51	0.43		[2, 3]
Licaria triandra		0.60	0.35		[2, 3]
Ligustrum sinense	-0.77	0.41	0.44	16.4	[1, 3, 9]
Ligustrum vulgare	-2.82	0.54		8.4	[1, 2]
Liquidambar styraciflua	-3.12	0.31	0.16	15.0	[1-3]
Liriodendron tulipifera	-3	0.27	0.14		[2, 3, 7]
Litsea leefeana		0.34	0.23		[5]
Lomatia myricoides		0.37	0.29		[5]
Lonchocarpus nelsii		0.51	0.60		[2, 3]
Lophira alata		0.52	0.32		[2, 3]
Lophopetalum subobovatum	-0.59	0.36		27.1	[1, 2]
Lophostemon suaveolens		0.37	0.27		[4]
Lovoa trichilioides		0.30	0.18		[2, 3]
Mabea nitida		0.47	0.39		[2, 3]
Macaranga denticulata	-1.14	0.31		21.7	[1, 2]
Machaerium villosum		0.57	0.38		[2, 3]
Maclura tinctoria		0.51	0.41		[2, 3]
Magnolia acuminata		0.29	0.14		[2, 3]
Magnolia virginiana		0.28	0.13		[2, 3]
Mallotus paniculatus	-1.32	0.23	0.29		[2, 3, 11]
Malus sylvestris	-6.01	0.41		11.2	[1, 2]
Manilkara bidentata	-2.70	0.56		26.1	[1, 2]
Mansonia altissima		0.37	0.24		[2, 3]
Margaritaria nobilis		0.60	0.37		[2, 3]
Melaleuca leucadendra		0.42	0.18		[2, 3]
Melaleuca nervosa		0.38	0.35		[5]
Melaleuca viridiflora		0.37	0.25		[5]
Melicope xanthoxyloides		0.29	0.31		[5]
Microberlinia brazzavillensis		0.44	0.32		[2, 3]
Milicia excelsa		0.37	0.32		[2, 3]
Millettia laurentii		0.50	0.50		[2, 3]
Mimosa scabrella		0.45	0.22		[2, 3]
Mimulus aurantiacus		0.41	0.45		[2, 3]

Minquartia guianensis		0.51	0.35		[2, 3]
Morisonia americana	-2.39	0.59		24.6	[1, 2]
Musanga cecropioides		0.26	0.24		[2, 3]
Musgravea heterophylla		0.30	0.47		[5]
Myrcia amazonica		0.55	0.37		[2, 3]
Myristica globosa		0.30	0.35		[5]
Nauclea diderrichii		0.42	0.29		[2, 3]
Nephelium lappaceum	-0.76	0.41		27.3	[1, 2]
Nerium oleander	-1.70	0.40		16.4	[1, 2]
Nesogordonia papaverifera		0.44	0.44		[2, 3]
Nyssa sylvatica	-1.82	0.31	0.13	15.0	[1-3]
Ochroma pyramidale	-1.00	0.09	0.92	28.3	[1-3]
Ocotea guianensis		0.42	0.25		[2, 3]
Olea europaea	-7.20	0.47		18.2	[1, 2]
Olearia megalophylla		0.41	0.21		[5]
Olearia phlogopappa		0.41	0.22		[5]
Ormosia coutinhoi		0.44	0.54		[2, 3]
Ormosia nobilis		0.39	0.51		[2, 3]
Ouratea hexasperma	-1.48	0.31		21	[1, 7]
Oxandra asbeckii		0.51	0.23		[2, 3]
Oxydendrum arboreum	-4.54	0.33		15	[1, 2]
Oxystigma oxyphyllum		0.34	0.29		[2, 3]
Ozothamnus secundiflorus		0.38	0.27		[5]
Pachira minor		0.37	0.50		[2, 3]
Palaquium galactoxylum		0.34	0.38		[5]
Parinari excelsa		0.43	0.44		[2, 3]
Parkia filicoidea		0.30	0.47		[2, 3]
Payena endertii	-0.63	0.45		27.1	[1, 2]
Peltogyne venosa		0.50	0.36		[2, 3]
Pericopsis elata		0.41	0.30		[2, 3]
Persoonia falcata		0.43	0.14		[4]
Persoonia juniperina		0.43	0.24		[4]
Persoonia subvelutina		0.37	0.20		[5]
Petersianthus macrocarpus		0.46	0.20		[2, 3]

Phillyrea angustifolia	-4.97	0.56		17.7	[6]
Photinia arbutifolia	-6.24	0.42			[1, 2]
Pimelea linifolia		0.29	0.12		[5]
Pimelea linifolia		0.33	0.17		[5]
Piptadeniastrum africanum		0.37	0.37		[2, 3]
Pistacia lentiscus	-4.79	0.53		18.1	[1, 7]
Pistacia terebinthus	-3.44	0.47		17.7	[6]
Pithecellobium dulce	-1.65	0.37		24.6	[1, 2]
Platanus acerifolia		0.37	0.40		[2, 3]
Polyscias sambucifolia		0.37	0.25		[5]
Populus balsamifera	-1.80	0.21		9.0	[1, 2]
Populus deltoides	-1.21	0.25	0.14	18.6	[1-3]
Populus grandidentata		0.24	0.11		[2, 3]
Populus nigra	-2.95	0.24		10.9	[1, 2]
Populus tremula	-1.30	0.26		8.4	[1, 2]
Populus tremuloides	-2.74	0.23		1.8	[1, 2]
Populus trichocarpa	-1.50	0.21		10.8	[1, 2]
Pourouma cecropiifolia		0.31	0.54		[2, 3]
Pouteria elegans		0.49	0.45		[2, 3]
Pouteria macrophylla		0.61	0.49		[2, 3]
Pouteria nemorosa		0.29	0.54		[2, 3]
Pouteria xerocarpa*		0.34	0.50		[5]
Prioria copaifera	-1.60	0.27		26.3	[1, 2]
Prosopis alpataco		0.46	0.48		[2, 3]
Prosopis glandulosa		0.47	0.62		[2, 3]
Protium opacum		0.38	0.11		[2, 3]
Protium panamense	-1.70	0.30		26.1	[1, 2]
Protium pittieri		0.32	0.29		[2, 3]
Prunus armeniaca	-6.07	0.45		10.6	[1, 2]
Prunus avium	-4.76	0.32	0.23	8.3	[1-3]
Prunus ilicifolia	-4.39	0.49		16.6	[1, 2]
Prunus mahaleb	-5.36	0.56		10.6	[6]
Prunus padus	-3.54	0.31		8.4	[1, 2]
Pseudobombax munguba		0.18	0.31		[2, 3]
Pseudobombax septenatum	-1.00	0.09		26.3	[1, 2]

Pseudolmedia laevis		0.42	0.51		[2, 3]
Pseudoxandra polyphleba		0.25	0.50		[2, 3]
Psidium acutangulum		0.65	0.38		[2, 3]
Pterocarpus angolensis		0.34	0.38		[2, 3]
Pterocarpus macrocarpus		0.47	0.29		[2, 3]
Pterocarpus soyauxii		0.39	0.36		[2, 3]
Pterygota macrocarpa		0.33	0.43		[2, 3]
Pycnanthus angolensis		0.25	0.38		[2, 3]
Pyrus communis		0.40	0.29		[2, 3]
Qualea parviflora	-1.65	0.32		21	[1, 7]
Quercus alba	-1.37	0.40	0.26	15.0	[1-3]
Quercus coccifera	-6.96	0.49		18.1	[1, 7]
Quercus coccinea		0.40	0.40		[2, 3]
Quercus falcata	-0.92	0.35	0.46	15.0	[1-3]
Quercus gambelii	-0.18	0.41		10.7	[1, 2]
Quercus garryana	-3.61	0.43	0.25		[2, 3, 7]
Quercus ilex	-4.97	0.59		9.4	[6]
Quercus laevis	-1.89	0.43		15.6	[1, 2]
Quercus laurifolia		0.37	0.41		[2, 3]
Quercus macrocarpa		0.39	0.33		[2, 3]
Quercus nigra	-1.31	0.37	0.43	15.0	[1-3]
Quercus oleoides	-3.03	0.57		26.0	[1, 2]
Quercus petraea	-3.50	0.37		9.4	[1, 2]
Quercus phellos	-1.42	0.37		15	[1, 2]
Quercus prinus	-1.70	0.38			[1, 2]
Quercus pubescens	-3.00	0.51		14.7	[6]
Quercus robur	-2.80	0.37	0.22	9.1	[1-3]
Quercus rubra	-1.61	0.37	0.14	15.0	[1-3]
Quercus shumardii		0.43	0.42		[2, 3]
Quercus stellata	-1.44	0.40	0.36	15.6	[1-3]
Quercus velutina	-2.53	0.37	0.43		[2, 3, 12]
Rapanea melanophloeos	-1.85	0.50		15.9	[1, 2]
Rhamnus californica	-2.51	0.33	0.11	14.6	[1-3]
Rhamnus crocea	-5.17	0.50	0.16	16.3	[1-3]
Rhamnus frangula	-2.92	0.33			[1, 2]

Rhamnus ilicifolia	-5.92	0.43	0.08	14.4	[1, 3, 7]
Rhizophora apiculata		0.57	0.19		[2, 3]
Rhizophora mangle	-6.30	0.59		25	[1, 2]
Rhododendron maximum	-2.20	0.38	0.20	13.7	[1, 3, 9]
Rhus laurina	-2.40	0.42			[1, 7]
Rhus trilobata	-2.95	0.50	0.22	14.6	[1, 3, 9]
Robinia pseudoacacia	-2.59	0.48	0.13	9.9	[1, 3, 6]
Rockinghamia angustifolia		0.30	0.33		[5]
Salix alba	-1.50	0.19		10.9	[1, 2]
Salix caprea	-1.90	0.26		8.4	[1, 2]
Salix fragilis	-1.39	0.24		10.9	[1, 2]
Salix nigra		0.24	0.08		[2, 3]
Salix purpurea	-1.97	0.31		8.4	[1, 2]
Salvia mellifera	-4.62	0.44	0.33	15.3	[1, 3, 9]
Salvia officinalis	-3.08	0.39			[6]
Sambucus caerulea	-1.43	0.31		6.6	[1, 2]
Sapindus saponaria		0.41	0.52		[2, 3]
Sapium glandulosum		0.30	0.39		[2, 3]
Sapium sebiferum	-1.37	0.32		17.1	[1, 2]
Schefflera macrocarpa	-1.72	0.37		21	[1, 7]
Schefflera morototoni	-1.38	0.27		26.9	[1, 2]
Schinopsis lorentzii		0.60	0.23		[2, 3]
Schinus terebinthifolius	-1.68	0.37		22.7	[1, 7]
Schizolobium parahyba		0.33	0.26		[2, 3]
Shorea faguetiana	-0.37	0.31		27.1	[1, 2]
Shorea hypochra		0.39	0.27		[2, 3]
Shorea mecistopteryx	-0.63	0.28		27.1	[1, 2]
Shorea obtusa		0.57	0.34		[2, 3]
Shorea ovalis	-0.39	0.30		27.1	[1, 2]
Simarouba amara		0.23	0.48	26.4	[2, 3]
Sindora leiocarpa	-0.86	0.32		27.3	[1, 2]
Sindoropsis letestui		0.37	0.24		[2, 3]
Sophora japonica	-2.60	0.40		10.0	[1, 2]
Sorbus aria	-5.38	0.45		8.4	[1, 2]
Sorbus aucuparia	-4.19	0.42	0.21	8.3	[1-3]

Sorbus torminalis	-4.11	0.55	0.25	10.9	[1, 3, 6]
Spartium junceum	-3.75	0.39			[6]
Staudtia kamerunensis		0.53	0.31		[2, 3]
Stemonurus umbellatus	-0.18	0.41		27.3	[1, 2]
Sterculia oblonga		0.41	0.49		[2, 3]
Sterculia rhinopetala		0.44	0.50		[2, 3]
Swartzia argentea		0.57	0.39		[2, 3]
Swartzia laevicarpa		0.43	0.47		[2, 3]
Swartzia polyphylla		0.41	0.49		[2, 3]
Swietenia macrophylla	-2.20	0.31	0.17	26.0	[1-3]
Symphonia globulifera		0.39	0.47		[2, 3]
Syzygium graveolens		0.36	0.44		[5]
Syzygium monospermum		0.41	0.52		[5]
Syzygium sayeri	-2.1	0.33	0.50		[5, 13]
Tabebuia ochracea		0.55	0.44		[2, 3]
Tachigali versicolor	-1.60	0.35		26.1	[1, 2]
Tapirira guianensis	-1.80	0.31		26.1	[1, 2]
Tectona grandis		0.34	0.18		[2, 3]
Terminalia amazonia		0.44	0.31		[2, 3]
Terminalia catappa		0.39	0.26		[2, 3]
Terminalia guyanensis		0.58	0.44		[2, 3]
Terminalia ivorensis		0.28	0.27		[2, 3]
Terminalia oblonga		0.45	0.52		[2, 3]
Terminalia sericea		0.48	0.33		[2, 3]
Terminalia superba		0.29	0.30		[2, 3]
Testulea gabonensis		0.39	0.26		[2, 3]
Tetraberlinia bifoliolata		0.31	0.20		[2, 3]
Tetracentron sinense	-1.42	0.22		13.8	[1, 2]
Tieghemella africana		0.40	0.35		[2, 3]
Tieghemella heckelii		0.34	0.40		[2, 3]
Tilia americana		0.21	0.08		[2, 3]
Tilia cordata	-1.65	0.28	0.17	9.5	[1, 3, 6]
Tilia platyphyllos	-3.09	0.28	0.12	8.3	[1-3]
Toechima erythrocarpum		0.38	0.21		[5]
Trattinnickia aspera	-1.10	0.28		26.1	[1, 2]

Trema micrantha		0.16	0.22		[2, 3]
Trichilia dregeana	-2.66	0.32		20.9	[1, 2]
Trichilia schomburgkii		0.45	0.26		[2, 3]
Triplaris americana		0.33	0.13		[2, 3]
Triplochiton scleroxylon		0.19	0.59		[2, 3]
Ulmus alata		0.40	0.30		[2, 3]
Ulmus americana		0.31	0.17		[2, 3]
Ulmus glabra	-0.50	0.37	0.20		[8]
Ulmus minor	-1.06	0.37	0.20		[8]
Ulmus rubra		0.32	0.13		[2, 3]
Ulmus thomasii		0.38	0.19		[2, 3]
Umbellularia californica	-1.35	0.34		16.0	[1, 2]
Viburnum lantana	-2.79	0.48		10.9	[1, 2]
Virola surinamensis		0.26	0.16		[2, 3]
Vitex cymosa		0.38	0.39		[2, 3]
Vochysia ferruginea	-1.00	0.30		26.1	[1, 2]
Vochysia tomentosa		0.24	0.38		[2, 3]
Wisteria sinensis	-1.19	0.41			[6]
Wrightia laevis		0.25	0.39		[5]
Xerospermum laevigatum	-0.18	0.51		27.3	[1, 2]
Ximenia americana		0.47	0.13		[2, 3]
Xylia xylocarpa		0.45	0.25		[2, 3]
Xylomelum scottianum		0.41	0.53		[5]
Zanthoxylum gilletii		0.43	0.21		[2, 3]
Zanthoxylum heitzii		0.32	0.18		[2, 3]

Table A.2. Biological data for 83 species of gymnosperm collected from literature study.[2]

Species	P_{50} [MPa]	η_w	η_p	MAT [°C]	Ref
Abies alba	-3.65	0.24	0.05	9.1	[1-3]
Abies amabilis		0.27	0.07		[2, 3]
Abies balsamea	-3.87	0.22	0.06	2.9	[1-3]
Abies concolor	-3.74	0.25	0.09	9.5	[1-3]
Abies grandis	-3.65	0.23	0.05	6.3	[1-3]
Abies lasiocarpa	-3.34	0.21			[1, 2]
Abies pinsapo	-4.15	0.27			[1, 2]
Abies procera		0.25	0.07		[2, 3]
Agathis australis	-2.58	0.30	0.07	14.5	[1-3]
Agathis borneensis	-1.91	0.27			[1, 2]
Araucaria angustifolia		0.31	0.06		[2, 3]
Araucaria hunsteinii	-4.07	0.26			[1, 2]
Austrocedrus chilensis	-9.95	0.28			[1, 2]
Callitris rhomboidea	-9.20	0.31			[1, 2]
Calocedrus decurrens	-7.75		0.09		[1, 3]
Cedrus atlantica	-4.50	0.29			[1, 2]
Cedrus deodara	-4.95	0.31			[1, 2]
Chamaecyparis lawsoniana	-5.17	0.26	0.06	15.0	[1-3]
Chamaecyparis thyoides		0.21	0.05		[2, 3]
Cryptomeria japonica	-4.55	0.31			[1, 2]
Cunninghamia lanceolata	-6.93	0.18			[1, 2]
Fitzroya cupressoides	-7.50	0.29	0.14	15.0	[1-3]
Ginkgo biloba	-4.62	0.31			[1, 2]
Glyptostrobus pensilis	-2.80	0.33			[1, 2]
Gnetum gnemon	-4.62	0.41			[1, 2]
Juniperus communis	-6.43	0.34			[1, 2]
Juniperus deppeana	-8.90	0.32			[1, 2]

[2] P_{50} is the pressure that causes cavitation to form so that the hydraulic conductivity of the stem is halved; η_w is wood fraction of sapwood, η_p is parenchyma fraction of sapwood; and MAT is mean annual temperature of the habitat.

Juniperus flaccida	-7.80		0.08		[1, 3]
Juniperus monosperma	-11.60	0.41			[1, 7]
Juniperus occidentalis	-9.00		0.07		[1, 3]
Juniperus thurifera		0.35	0.07		[2, 3]
Juniperus virginiana	-6.60	0.29	0.06	17.0	[1-3]
Larix decidua	-3.66	0.32	0.06	8.9	[1-3]
Larix kaempferi	-3.43	0.28			[1, 2]
Larix laricina		0.33	0.11		[2, 3]
Larix occidentalis	-4.31	0.32	0.10	2.4	[1-3]
Metasequoia glyptostroboides	-3.76	0.20			[1, 2]
Phyllocladus trichomanoides	-7.02	0.35			[1, 2]
Picea abies	-3.98	0.25	0.05	0.0	[1-3]
Picea engelmannii	-4.91	0.22	0.06	2.0	[1-3]
Picea glauca	-4.30	0.22	0.07	2.9	[1-3]
Picea mariana	-5.30	0.25			[1, 2]
Picea rubens	-3.53	0.25	0.05	6.8	[1-3]
Picea sitchensis	-3.85	0.25	0.07	8.7	[1-3]
Pinus banksiana		0.27	0.08		[2, 3]
Pinus canariensis		0.41	0.13		[2, 3]
Pinus caribaea	-3.27	0.34			[1, 2]
Pinus cembra	-3.34		0.09		[1, 3]
Pinus contorta	-3.67	0.25	0.06	8.0	[1-3]
Pinus echinata	-3.21	0.31	0.08	15.0	[1-3]
Pinus edulis	-4.88	0.33			[1, 2]
Pinus elliottii		0.36	0.12		[2, 3]
Pinus flexilis	-3.71	0.25			[1, 2]
Pinus halepensis	-3.11	0.31			[1, 2]
Pinus jeffreyi		0.25	0.08		[2, 3]
Pinus kesiya		0.30	0.05		[2, 3]
Pinus lambertiana		0.23	0.06		[2, 3]
Pinus massoniana		0.31	0.08		[2, 3]
Pinus merkusii		0.35	0.08		[2, 3]
Pinus monticola		0.23	0.07		[2, 3]
Pinus nigra	-2.80	0.28	0.05	12.8	[1-3]
Pinus pinaster	-3.01	0.28	0.06	10.9	[1-3]

Pinus pinea	-3.65	0.33			[1, 2]
Pinus ponderosa	-2.65	0.25	0.07	-0.3	[1-3]
Pinus radiata		0.26	0.11		[2, 3]
Pinus resinosa		0.27	0.07		[2, 3]
Pinus rigida		0.31	0.07		[2, 3]
Pinus strobus		0.23	0.04		[2, 3]
Pinus sylvestris	-3.61	0.28	0.06	10.9	[1-3]
Pinus taeda	-3.13	0.31	0.08	15.0	[1-3]
Pinus uncinata	-4.18	0.27			[1, 2]
Pinus virginiana		0.30	0.07		[2, 3]
Podocarpus latifolius	-1.74	0.31			[1, 2]
Podocarpus oleifolius		0.31	0.07		[2, 3]
Sequoia sempervirens	-6.75	0.25	0.08	15.0	[1-3]
Taxodium distichum	-2.14	0.28	0.07	15.6	[1-3]
Taxus baccata	-8.14	0.37	0.14	15.0	[1-3]
Taxus brevifolia	-6.44	0.40			[1, 2]
Tetraclinis articulata	-8.55	0.48			[1, 2]
Thuja occidentalis	-3.57	0.19	0.03	7.4	[1-3]
Thuja plicata	-5.27	0.21	0.07	15.0	[1-3]
Tsuga canadensis	-3.07	0.25	0.06	7.4	[1-3]
Tsuga heterophylla	-3.1	0.28	0.09		[2, 3, 7]

[1] Choat, B., Jansen, S., Brodribb, T. J., Cochard, H., Delzon, S., Bhaskar, R., . . . Zanne, A. E. (2012). Global convergence in the vulnerability of forests to drought. Nature, 491(7426), 752-755. doi:10.1038/nature11688

[2] Chave, J., Coomes, D., Jansen, S., Lewis, S. L., Swenson, N. G., & Zanne, A. E. (2009). Towards a worldwide wood economics spectrum. Ecol Lett, 12(4), 351-366. doi:10.1111/j.1461-0248.2009.01285.x

[3] Morris, H., Plavcova, L., Cvecko, P., Fichtler, E., Gillingham, M. A. F., Martinez-Cabrera, H. I., . . . Jansen, S. (2016). A global analysis of parenchyma tissue fractions in secondary xylem of seed plants. New

Phytologist, 209(4), 1553-1565. doi:10.1111/nph.13737

[4] Ziemińska, K., Butler, D. W., Gleason, S. M., Wright, I. J., & Westoby, M. (2013). Fibre wall and lumen fractions drive wood density variation across 24 Australian angiosperms. AoB PLANTS, 5, plt046-plt046. doi:10.1093/aobpla/plt046

[5] Zieminska, K., Westoby, M., & Wright, I. J. (2015). Broad Anatomical Variation within a Narrow Wood Density Range-A Study of Twig Wood across 69 Australian Angiosperms. PLoS One, 10(4), 25. doi:10.1371/journal.pone.0124892

[6] Savi, T., Tintner, J., Da Sois, L., Grabner, M., Petit, G., & Rosner, S. (2018). The potential of Mid-Infrared spectroscopy for prediction of wood density and vulnerability to embolism in woody angiosperms. Tree Physiology.

[7] Fu, X., & Meinzer, F. C. (2018). Metrics and proxies for stringency of regulation of plant water status (iso/anisohydry): a global data set reveals coordination and trade-offs among water transport traits. Tree Physiology, tpy087-tpy087. doi:10.1093/treephys/tpy087

[8] Pausas, J. G., Pratt, R. B., Keeley, J. E., Jacobsen, A. L., Ramirez, A. R., Vilagrosa, A., . . . Davis, S. D. (2016). Towards understanding resprouting at the global scale. New Phytologist, 209(3), 945-954. doi:doi:10.1111/nph.13644

[9] Martinez-Cabrera, H. I., Jones, C. S., Espino, S., & Schenk, H. J. (2009). WOOD ANATOMY AND WOOD DENSITY IN SHRUBS: RESPONSES TO VARYING ARIDITY ALONG TRANSCONTINENTAL TRANSECTS. American Journal of Botany, 96(8), 1388-1398. doi:10.3732/ajb.0800237

[10] Jacobsen, A. L., Ewers, F. W., Pratt, R. B., Paddock, W. A., & Davis, S. D. (2005). Do xylem fibers affect vessel cavitation resistance? Plant Physiol, 139(1), 546-556. doi:10.1104/pp.104.058404

[11] ZHU, S.-D., SONG, J.-J., LI, R.-H., & YE, Q. (2013). Plant hydraulics and photosynthesis of 34 woody species from different successional stages of subtropical forests. Plant, Cell & Environment, 36(4), 879-891. doi:doi:10.1111/pce.12024

References

Barigah, T. S., Charrier, O., Douris, M., Bonhomme, M., Herbette, S., Ameglio, T., . . . Cochard, H. (2013). Water stress-induced xylem hydraulic failure is a causal factor of tree mortality in beech and poplar. Ann Bot, 112(7), 1431-1437. doi:10.1093/aob/mct204

Berthier, E., Young, E. W. K., & Beebe, D. (2012). Engineers are from PDMS-land, Biologists are from Polystyrenia. Lab Chip, 12(7), 1224-1237. doi:10.1039/c2lc20982a

Braun, H. (1984). The significance of the accessory tissues of the hydrosystem for osmotic water shifting as the second principle of water ascent, with some thoughts concerning the evolution of trees. IAWA Journal, 5(4), 275-294.

Brodersen, C. R., & McElrone, A. J. (2013). Maintenance of xylem network transport capacity: a review of embolism repair in vascular plants. Front Plant Sci, 4, 11. doi:10.3389/fpls.2013.00108

Brodribb, T. J. (2009). Xylem hydraulic physiology: The functional backbone of terrestrial plant productivity. Plant Science, 177(4), 245-251. doi:10.1016/j.plantsci.2009.06.001

Chave, J., Coomes, D., Jansen, S., Lewis, S. L., Swenson, N. G., & Zanne, A. E. (2009). Towards a worldwide wood economics spectrum. Ecol Lett, 12(4), 351-366. doi:10.1111/j.1461-0248.2009.01285.x

Choat, B., Brodribb, T. J., Brodersen, C. R., Duursma, R. A., López, R., & Medlyn, B. E. (2018). Triggers of tree mortality under drought. Nature,

558(7711), 531-539. doi:10.1038/s41586-018-0240-x

Choat, B., Jansen, S., Brodribb, T. J., Cochard, H., Delzon, S., Bhaskar, R., . . . Zanne, A. E. (2012). Global convergence in the vulnerability of forests to drought. Nature, 491(7426), 752-755. doi:10.1038/nature11688

De Gennes, P.-G., Brochard-Wyart, F., & Quéré, D. (2013). Capillarity and wetting phenomena: drops, bubbles, pearls, waves: Springer Science & Business Media.

Debenedetti, P. G. (1996). Metastable liquids: concepts and principles: Princeton University Press.

Dixon, H. H., & Joly, J. (1894). On the ascent of sap. Proceedings of the Royal Society of London, 57(340-346), 3-5.

Fornasiero, F., Tang, D., Boushehri, A., Prausnitz, J., & Radke, C. J. (2008). Water diffusion through hydrogel membranes - A novel evaporation cell free of external mass-transfer resistance. Journal of Membrane Science, 320(1-2), 423-430. doi:10.1016/j.memsci.2008.04.032

Fu, X., & Meinzer, F. C. (2018). Metrics and proxies for stringency of regulation of plant water status (iso/anisohydry): a global data set reveals coordination and trade-offs among water transport traits. Tree Physiology, tpy087-tpy087. doi:10.1093/treephys/tpy087

Hacke, U. G., Sperry, J. S., Pockman, W. T., Davis, S. D., & McCulloch, K. A. (2001). Trends in wood density and structure are linked to prevention of xylem implosion by negative pressure. Oecologia, 126(4), 457-461. doi:10.1007/s004420100628

Hartmann, H., & Trumbore, S. (2016). Understanding the roles of nonstructural carbohydrates in forest trees - from what we can measure to

what we want to know. New Phytologist, 211(2), 386-403. doi:10.1111/nph.13955

Herbert, E., Balibar, S., & Caupin, F. (2006). Cavitation pressure in water. Phys Rev E Stat Nonlin Soft Matter Phys, 74(4 Pt 1), 041603. doi:10.1103/PhysRevE.74.041603

Jacobsen, A. L., Ewers, F. W., Pratt, R. B., Paddock, W. A., & Davis, S. D. (2005). Do xylem fibers affect vessel cavitation resistance? Plant Physiol, 139(1), 546-556. doi:10.1104/pp.104.058404

Jacobsen, A. L., Pratt, R. B., Ewers, F. W., & Davis, S. D. (2007). Cavitation resistance among 26 chaparral species of southern California. Ecological Monographs, 77(1), 99-115.

Jensen, K. H., Berg-Sorensen, K., Bruus, H., Holbrook, N. M., Liesche, J., Schulz, A., . . . Bohr, T. (2016). Sap flow and sugar transport in plants. Reviews of Modern Physics, 88(3), 63. doi:10.1103/RevModPhys.88.035007

Johnson, D. M., McCulloh, K. A., Woodruff, D. R., & Meinzer, F. C. (2012). Hydraulic safety margins and embolism reversal in stems and leaves: Why are conifers and angiosperms so different? Plant Science, 195, 48-53. doi:10.1016/j.plantsci.2012.06.010

Kitin, P., Voelker, S. L., Meinzer, F. C., Beeckman, H., Strauss, S. H., & Lachenbruch, B. (2010). Tyloses and phenolic deposits in xylem vessels impede water transport in low-lignin transgenic poplars: a study by cryo-fluorescence microscopy. Plant Physiol, 154(2), 887-898.

Labarbera, M. (1990). PRINCIPLES OF DESIGN OF FLUID TRANSPORT-SYSTEMS IN ZOOLOGY. Science, 249(4972), 992-1000. doi:10.1126/science.2396104

Martinez-Cabrera, H. I., Jones, C. S., Espino, S., & Schenk, H. J. (2009). WOOD ANATOMY AND WOOD DENSITY IN SHRUBS: RESPONSES TO VARYING ARIDITY ALONG TRANSCONTINENTAL TRANSECTS. American Journal of Botany, 96(8), 1388-1398. doi:10.3732/ajb.0800237

McCulloh, K. A., Sperry, J. S., & AdlerO, F. R. (2004). Murray's law and the hydraulic vs mechanical functioning of wood. Functional Ecology, 18(6), 931-938. doi:10.1111/j.0269-8463.2004.00913.x

Moles, A. T., Perkins, S. E., Laffan, S. W., Flores- Moreno, H., Awasthy, M., Tindall, M. L., . . . Aarssen, L. W. (2014). Which is a better predictor of plant traits: temperature or precipitation? Journal of Vegetation Science, 25(5), 1167-1180.

Morris, H., Plavcova, L., Cvecko, P., Fichtler, E., Gillingham, M. A. F., Martinez-Cabrera, H. I., . . . Jansen, S. (2016). A global analysis of parenchyma tissue fractions in secondary xylem of seed plants. New Phytologist, 209(4), 1553-1565. doi:10.1111/nph.13737

Nardini, A., Lo Gullo, M. A., & Salleo, S. (2011). Refilling embolized xylem conduits: Is it a matter of phloem unloading? Plant Science, 180(4), 604-611. doi:10.1016/j.plantsci.2010.12.011

Nobel, P. S. (1983). Biophysical plant physiology and ecology: WH Freeman and company.

Nobel, P. S. (1991). Achievable productivities of certain CAM plants: basis for high values compared with C3 and C4 plants. New Phytologist, 119(2), 183-205.

Noblin, X., Mahadevan, L., Coomaraswamy, I. A., Weitz, D. A., Holbrook, N. M., & Zwieniecki, M. A. (2008). Optimal vein density in artificial and real

leaves. Proc Natl Acad Sci U S A, 105(27), 9140-9144. doi:10.1073/pnas.0709194105

Pausas, J. G., Pratt, R. B., Keeley, J. E., Jacobsen, A. L., Ramirez, A. R., Vilagrosa, A., . . . Davis, S. D. (2016). Towards understanding resprouting at the global scale. New Phytologist, 209(3), 945-954. doi:doi:10.1111/nph.13644

Piquemal, J., Lapierre, C., Myton, K., O'connell, A., Schuch, W., Grima-pettenati, J., & Boudet, A.-M. (1998). Down-regulation of Cinnamoyl-CoA Reductase induces significant changes of lignin profiles in transgenic tobacco plants. The Plant Journal, 13(1), 71-83. doi:doi:10.1046/j.1365-313X.1998.00014.x

Pratt, R. B., Jacobsen, A. L., Ewers, F. W., & Davis, S. D. (2007). Relationships among xylem transport, biomechanics and storage in stems and roots of nine Rhamnaceae species of the California chaparral. New Phytologist, 174(4), 787-798. doi:10.1111/j.1469-8137.2007.02061.x

Savi, T., Tintner, J., Da Sois, L., Grabner, M., Petit, G., & Rosner, S. (2018). The potential of Mid-Infrared spectroscopy for prediction of wood density and vulnerability to embolism in woody angiosperms. Tree Physiology.

Sperry, J. S., Hacke, U. G., & Pittermann, J. (2006). Size and function in conifer tracheids and angiosperm vessels. American Journal of Botany, 93(10), 1490-1500.

Spicer, R. (2014). Symplasmic networks in secondary vascular tissues: parenchyma distribution and activity supporting long-distance transport. Journal of Experimental Botany, 65(7), 1829-1848. doi:10.1093/jxb/ert459

Vargaftik, N., Volkov, B., & Voljak, L. (1983). International tables of the

surface tension of water. Journal of Physical and Chemical Reference Data, 12(3), 817-820.

Venturas, M. D., Sperry, J. S., & Hacke, U. G. (2017). Plant xylem hydraulics: what we understand, current research, and future challenges. J Integr Plant Biol, 59(6), 356-389.

Vincent, O., Marmottant, P., Quinto-Su, P. A., & Ohl, C. D. (2012). Birth and growth of cavitation bubbles within water under tension confined in a simple synthetic tree. Phys Rev Lett, 108(18), 184502. doi:10.1103/PhysRevLett.108.184502

Vincent, O., Szenicer, A., & Stroock, A. D. (2016). Capillarity-driven flows at the continuum limit. Soft Matter, 12(31), 6656-6661. doi:10.1039/c6sm00733c

Wang, Z., Volinsky, A. A., & Gallant, N. D. (2014). Crosslinking effect on polydimethylsiloxane elastic modulus measured by custom- built compression instrument. Journal of Applied Polymer Science, 131(22).

Wheeler, T. D., & Stroock, A. D. (2008). The transpiration of water at negative pressures in a synthetic tree. Nature, 455(7210), 208-212. doi:10.1038/nature07226

Young, W. C., Budynas, R. G., & Sadegh, A. M. (2002). Roark's formulas for stress and strain (Vol. 7): McGraw-Hill New York.

ZHU, S.-D., SONG, J.-J., LI, R.-H., & YE, Q. (2013). Plant hydraulics and photosynthesis of 34 woody species from different successional stages of subtropical forests. Plant, Cell & Environment, 36(4), 879-891. doi:doi:10.1111/pce.12024

Ziemińska, K., Butler, D. W., Gleason, S. M., Wright, I. J., & Westoby, M.

(2013). Fibre wall and lumen fractions drive wood density variation across 24 Australian angiosperms. AoB PLANTS, 5, plt046-plt046. doi:10.1093/aobpla/plt046

Zieminska, K., Westoby, M., & Wright, I. J. (2015). Broad Anatomical Variation within a Narrow Wood Density Range-A Study of Twig Wood across 69 Australian Angiosperms. PLoS One, 10(4), 25. doi:10.1371/journal.pone.0124892

Zwieniecki, M. A., & Holbrook, N. M. (2009). Confronting Maxwell's demon: biophysics of xylem embolism repair. Trends Plant Sci, 14(10), 530-534. doi:10.1016/j.tplants.2009.07.002

국 문 초 록

나무 물관 내부 공동 현상에 대한 유체역학적 분석

서울대학교 공과대학원

기계항공공학부

최 진 우

건조한 환경은 식물에게 치명적이다. 물이 충분히 공급되지 못하면 줄기 내부에 기포가 형성되어 물관을 막는다. 이를 색전증이라고 한다. 이 때, 잎의 엽육 세포를 적시지 못해 생존할 수 없다. 색전증의 진행 과정은 이미 기체로 가득 찬 물관 요소에서 인접한 물관 요소로 기포가 전파되는 과정과 이 기포가 성장하며 물관 요소를 가득 채우는 과정으로 분리할 수 있다. 본 연구에서는 인공 식물을 제작하여 기포의 전파 및 성장을 실험적으로 분석하고, 이 결과를 실제 식물에 적용하였다.

인공 식물이란 특정 부피의 물을 다공성 구조가 둘러싸고 있는 형태이다. 다공성 구조 내부에 걸린 물의 계면은 인공 식물 내부 물을 잡아당기며 장력이 형성된다. 장력의 크기가 역치

이상으로 증가하면 기포가 형성된다. 실험적 결과는 1) 인공 식물 내부 물의 부피가 증가할수록 기포가 형성될 때까지 인공 식물의 부피 변화가 크다. 즉 인공 식물의 캐패시턴스가 증가한다. 2) 온도가 감소할수록 기포가 형성되는 역치가 증가한다. 그로 인하여 외부와의 압력차가 증가해 박막의 파열이 관찰된다. 3) 역치 압력이 0에 가까운 기포는 느리고 일정한 속력으로 성장한다. 4) 역치 압력이 큰 기포는 초기 속력이 빠르지만 감속한다.

식물 줄기의 기포 저항성은 줄기의 해부학적 구조에 따라 결정된다. 본 연구에서는 줄기의 구성 요소를 목질, 유조직, 빈 공간으로 나누었다. 빈 공간의 비율과 기포 저항성에 대하여 비교 연구를 수행한 결과 1) 빈 공간의 비율이 작을수록 캐패시턴스가 감소하여 기포가 빠르게 형성되어 기포 저항성이 감소한다. 2) 빈 공간의 비율이 클수록 물관벽에 파열이 일어날 가능성이 커져서 기포 저항성이 감소한다. 3) 이러한 두 한계는 침엽수와 활엽수에 구분되어 나타난다. 활엽수는 고온의 환경에서 서식하기 때문에 기포가 빈번히 발생할 수 있고, 유조직 세포의 비율을 높여서 색전증에 대응한다. 침엽수는 저온의 환경에서 서식하기 때문에 기포가 덜 형성되는 대신 큰 압력차로 물관벽에 파열이 일어날 수 있다. 침엽수는 이를 대비하여 물관벽의 강도를 높인다.

주요어 : 공동 현상, 색전증, 파열, 기포 저항성

학 번 : 2014-21843